Check for updates

JGR Atmospheres

RESEARCH ARTICLE
10.1029/2022JD038200

Evaluating ENSO's Spatiotemporal Complexity in the CWB CFS 1-Tiered Model Hindcasts

Ji-Won Kim[1], Ting-Huai Chang[2], Ching-Teng Lee[2], and Jin-Yi Yu[1]

[1]Department of Earth System Science, University of California, Irvine, CA, USA, [2]Central Weather Bureau, Taipei, Taiwan

Key Points:

- A coupled atmosphere-ocean model's ability to forecast spatiotemporal complexity in ENSO is evaluated by analyzing its hindcasts
- The EP type of ENSO is the most difficult to hindcast due to the model's warm bias in the tropical eastern Pacific that degrades amplitude forecasts
- Multi-year El Niño is more difficult to hindcast than multi-year La Niña due to the model's cold bias in the tropical central Pacific

Correspondence to:
J.-Y. Yu,
jyyu@uci.edu

Citation:
Kim, J.-W., Chang, T.-H., Lee, C.-T., & Yu, J.-Y. (2023). Evaluating ENSO's spatiotemporal complexity in the CWB CFS 1-tiered model hindcasts. *Journal of Geophysical Research: Atmospheres*, *128*, e2022JD038200. https://doi.org/10.1029/2022JD038200

Received 16 NOV 2022
Accepted 5 JUL 2023

Author Contributions:
Conceptualization: Ji-Won Kim, Jin-Yi Yu
Data curation: Ji-Won Kim, Ting-Huai Chang, Ching-Teng Lee
Formal analysis: Ji-Won Kim
Funding acquisition: Jin-Yi Yu
Investigation: Ji-Won Kim
Methodology: Ji-Won Kim, Jin-Yi Yu
Software: Ji-Won Kim
Supervision: Jin-Yi Yu
Validation: Ji-Won Kim, Jin-Yi Yu
Writing – original draft: Ji-Won Kim
Writing – review & editing: Ji-Won Kim, Ting-Huai Chang, Ching-Teng Lee, Jin-Yi Yu

© 2023. American Geophysical Union. All Rights Reserved.

Abstract Using hindcasts produced by a coupled climate model, this study evaluates whether the model can forecast the observed spatiotemporal complexity in the El Niño–Southern Oscillation (ENSO) during the period 1982–2011: the eastern Pacific (EP), central Pacific-I (CP-I) and -II (CP-II) types of El Niño, and the multi-year evolution events of El Niño occurred in 1986–1988 (i.e., 1986/87/88 El Niño) and La Niña occurred in 1998–2000 (i.e., 1998/99/00 La Niña). With regard to the spatial complexity, it is found that the CP-I type of El Niño is the easiest to hindcast, the CP-II is second, and the EP is most difficult to hindcast as its amplitude is significantly underestimated in the model used here. The model deficiency in hindcasting the EP El Niño is related to a warm bias in climatological sea surface temperatures (SSTs) in the tropical eastern Pacific. This warm bias is related to model biases in the strengths of the Pacific Walker circulation and South Pacific high, both of which are notably weaker than observed. As for the temporal complexity, the model successfully hindcasts the multi-year evolution of the 1998/99/00 La Niña but fails to accurately hindcast the 1986/87/88 El Niño. This contrasting model performance in hindcasting multi-year events is found to be related to a cold bias in climatological SSTs in the tropical central Pacific. This cold bias result enables the model La Niña, but not El Niño, to activate intrabasin tropical–subtropical interactions associated with the Pacific Meridional Mode that produce the multi-year evolution pattern.

Plain Language Summary The El Niño–Southern Oscillation (ENSO) events differ considerably from one event to another. These differences commonly appear in its spatial structure (three different types of El Niño as EP, CP-I, and CP-II types) and temporal evolution (single-vs. multi-year evolution types). By evaluating climate model hindcasts of these different spatiotemporal types of events during the period 1982–2011, this study finds that the CP-I El Niño is the easiest to hindcast, followed by the CP-II El Niño, while the EP El Niño is the most difficult to hindcast. In addition, it is found that the model has a better hindcast performance for single-year events than multi-year ones and is better able to hindcast multi-year La Niña than multi-year El Niño. The warm and cold biases in the model that impair the model's ability to hindcast the different sorts of ENSO are also identified. The findings of this study will benefit the ENSO forecast and climate model communities.

1. Introduction

It is being increasingly recognized that the El Niño–Southern Oscillation (ENSO) has considerable complexity in its properties (e.g., Timmermann et al., 2018). The complexity appears in both the spatial structure and temporal evolution of El Niño and La Niña (An et al., 2020; Capotondi et al., 2015; Kao & Yu, 2009; Kim & Yu, 2022; Timmermann et al., 2018; Wang et al., 2017; Yeh et al., 2014; Yu et al., 2017). Concerning the spatial complexity, some El Niños, such as the 1982/83 and 1997/98 events, are characterized by sea surface temperature (SST) anomalies that are largest in the tropical eastern Pacific, while others, like the 2002/03 and 2009/10 events, have their largest SST anomalies primarily confined to the tropical central Pacific. This structural diversity among El Niño events, often referred to as ENSO diversity (sometimes also called ENSO flavors), led to a categorization of El Niños into two different types: the Eastern Pacific (EP) El Niño and the Central Pacific (CP) El Niño (Kao & Yu, 2009; Yu & Kao, 2007). During its onset, development, and mature stages, the EP El Niño is generally characterized by maximum SST anomalies that are located in the tropical eastern Pacific, close to the South American coast (Figure 1a). The CP El Niño, however, has its maximum SST anomalies mostly in the tropical central Pacific, near the International Dateline (Figures 1b and 1c). The CP El Niño has occurred more frequently than the EP El Niño since the 1990s (Lee & McPhaden, 2010; Yu et al., 2012a) and is also known to have its own generation mechanism (Kao & Yu, 2009; Kug et al., 2009; Yeh et al., 2015; Yu et al., 2010; Yu & Kim, 2011). In

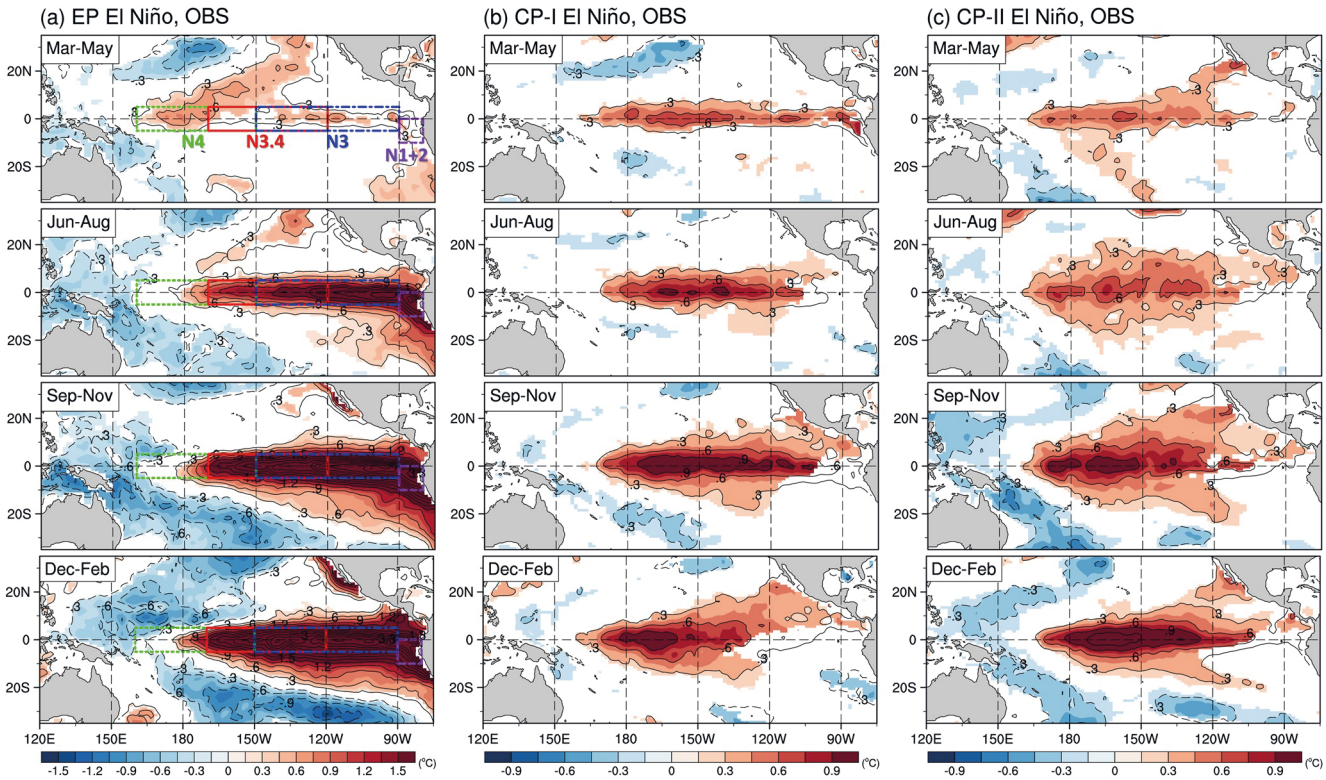

Figure 1. Composites of SST anomalies (in °C) over the tropical Pacific for (a) EP El Niño, (b) CP-I El Niño, and (c) CP-II El Niño from the observations during their developing spring (March−May), summer (June−August), fall (September−November), and peak winter (December−February). Only statistically significant anomalies (as determined using a bootstrap test are shown by the shaded areas (see Section 2). In (a), the various regions used to define Niño indices are denoted by rectangles where the green dotted line for the Niño4 (5°S−5°N, 160°E−150°W) index, the red solid line for the Niño3.4 (5°S−5°N, 190−120°W) index, the blue dashed-single dotted line for the Niño3 (5°S−5°N, 150−90°W) index, and the purple dash-double dotted line for the Niño1+2 (10°S−0, 90−80°W) index.

addition, its global climate impacts (H. M. Kim et al., 2009; Weng et al., 2009; Yu et al., 2012b; Yu & Zou, 2013) are also profoundly different from those of the EP El Niño.

More recent studies (Wang & Wang, 2013, 2014; Tan et al., 2016; Chen et al., 2019, 2021a; J. W. Kim et al., 2021) have even suggested that the CP El Niño can be further divided into two subtypes based on their different generation mechanisms and distinct climate impacts, which will be referred to as CP-I and CP-II El Niños in this study. The CP-I El Niño is characterized by warm SST anomalies that initially develop in the tropical central Pacific, with a structure that is aligned with the equator (Figure 1b). On the other hand, the CP-II El Niño is characterized by warm SST anomalies that first appear in the subtropical northeastern Pacific and then extend southwestward with an asymmetric structure about the equator (Figure 1c). Moreover, the warm anomalies associated with the CP-II El Niño tend to be located somewhat further west than those of the CP-I El Niño (cf. Figures 1b and 1c; see also Figure 4 in Wang & Wang, 2013). These structural differences between the CP-I and CP-II El Niños, despite their subtlety, can result in a variety of distinct climate impacts including rainfall amounts in southern China, typhoon tracks over the western North Pacific (Wang & Wang, 2013), and SST variations in the tropical Indian Ocean (Wang & Wang, 2014) and the South China Sea (Tan et al., 2016), strengths and locations of the western Pacific subtropical high (Chen et al., 2019, 2021a; Tan et al., 2016), and responses of the East Asian winter monsoon (J. W. Kim et al., 2021). Previous studies have also suggested that these two subtypes of the CP El Niño differ not only in their spatial structures and temporal evolutions but also in their underlying dynamics (Chen et al., 2021b and references therein). While the generation process of the CP-I El Niño is related to the Australian winter monsoon forcing via the Indonesian Throughflow and a subsurface thermocline mechanism, the generation process of the CP-II El Niño is associated with subtropical North Pacific forcing via the Pacific Meridional Mode (PMM) and a surface coupling mechanism. Those studies have used both observational/reanalysis products as well as climate model simulations.

Meanwhile, researchers have also recognized that there is significant complexity in the temporal evolution of ENSO (Fang & Yu, 2020b; Kim & Yu, 2020, 2021, 2022; X. Wu, Juang, et al., 2019; Yu & Fang, 2018). Some

21698996, 2023, 14, Downloaded from https://agupubs.onlinelibrary.wiley.com/doi/10.1029/2022JD038200 by University Of California - Irvine, Wiley Online Library on [21/08/2023]. See the Terms and Conditions (https://onlinelibrary.wiley.com/terms-and-conditions) on Wiley Online Library for rules of use; OA articles are governed by the applicable Creative Commons License

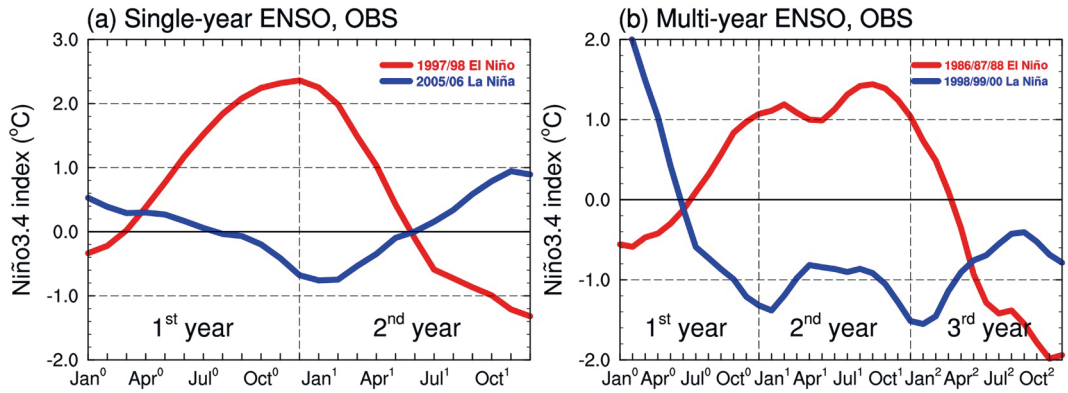

Figure 2. (a) Temporal evolutions of the observed Niño3.4 index for the single-year ENSO events of 1997/98 (El Niño, red curve) and 2005/06 (La Niña, blue curve). (b) Same as (a) except for the multi-year ENSO events of 1986–88 (El Niño, red curve) and 1998–2000 (La Niña, blue curve).

ENSO events, after reaching their mature stage, subsequently transition rapidly into a neutral condition or opposite ENSO phase, resulting in a single-year evolution pattern. Two examples of such single-year ENSO events are the 1997/98 El Niño and 2005/06 La Niña (Figure 2a). Some other ENSO events, however, do not transition to the opposite phase after their mature stage. They, instead, linger in the same phase and decay slowly during the second year, producing a multi-year evolution pattern. During some of these events a re-intensification can take place during the second year; the 1986/87/88 El Niño and 1998/99/00 La Niña (Figure 2b) are example of this sort of event. Recent studies have started to look into the physical mechanisms behind the multi-year evolution pattern, though with a greater focus on multi-year La Niña events (An & Kim, 2017, 2018; Choi et al., 2013; DiNezio & Deser, 2014; Dommenget et al., 2013; Hu et al., 2014; McGregor et al., 2012; Ohba & Ueda, 2009; Okumura et al., 2011). This is mainly because, on average, La Niña events last longer than El Niño events and more often evolve into multi-year events. However, it has been observed that multi-year El Niño events have been occurring more frequently during the 21st century than during the twentieth century. While the two extreme El Niños in the twentieth century (i.e., 1982/83 and 1997/98 events) were both single-year events, the extreme El Niño in the 21st century (i.e., 2015/16 event) was a multi-year evolution event preceded by a weak El Niño in 2014/15 (cf. Kim & Yu, 2020). Even more surprisingly, the next El Niño after the 2015/16 event was another multi-year El Niño that occurred from 2018 through 2020 (see website: https://origin.cpc.ncep.noaa.gov/products/analysis_monitoring/ensostuff/ONI_v5.php). Thus, it is increasingly important to gain a better understanding of ENSO's temporal complexity as it will ultimately help improve ENSO predictions, which are now limited to lead times of up to approximately 1 year (Barnston et al., 2019; X. Wu et al., 2021). Enhancing the predictability of ENSO's temporal complexity would also aid in preparation for ENSO-driven climate impacts that can vary highly depending upon whether an ENSO event is a single- or multi-year event (e.g., Iwakiri & Watanabe, 2020; Okumura et al., 2017; Paek et al., 2017).

Given the great importance of ENSO's spatiotemporal complexity, in this study we systematically examine observational data and climate model hindcast simulations to extend our understanding of how well and why climate models can or cannot properly forecast the spatiotemporal complexity of ENSO. To achieve this purpose, we specifically choose to analyze the (a) three types of El Niño (to address the spatial complexity) and (b) two multi-year events (to address the temporal complexity). The remainder of the paper is organized as follows. A detailed description of the observational/reanalysis datasets, climate model hindcast outputs, and analysis methodologies used in this study is provided in Section 2. In Section 3, by comparing the observational data and model hindcast outputs, we evaluate the model's ability to hindcast the observed ENSO spatiotemporal complexity into two subsections: Sections 3.1 and 3.2. The model deficiencies that lead to errors in the model hindcasts of the spatiotemporal complexity of ENSO are also identified. A summary and discussion of the main findings of this study are given in Section 4.

2. Data and Methods

Three monthly mean observational/reanalysis datasets were utilized in this study. Monthly mean SSTs from the Hadley Center Sea Ice and Sea Surface Temperature, version 1.1 (HadISSTv1.1; Rayner et al., 2003) are used.

21698996, 2023, 14, Downloaded from https://agupubs.onlinelibrary.wiley.com/doi/10.1029/2022JD038200 by University Of California - Irvine, Wiley Online Library on [21/08/2023]. See the Terms and Conditions (https://onlinelibrary.wiley.com/terms-and-conditions) on Wiley Online Library for rules of use; OA articles are governed by the applicable Creative Commons License

21698996, 2023, 14, Downloaded from https://agupubs.onlinelibrary.wiley.com/doi/10.1029/2022JD038200 by University Of California - Irvine, Wiley Online Library on [21/08/2023]. See the Terms and Conditions (https://onlinelibrary.wiley.com/terms-and-conditions) on Wiley Online Library for rules of use; OA articles are governed by the applicable Creative Commons License

The HadISSTv1.1 data has a horizontal resolution of 1.0° × 1.0° and covers the period from 1871 to the present. Monthly means of atmospheric variables including surface pressure (P_s) and the zonal (U) and meridional (V) wind components at 850-hPa level were provided by the National Centers for Environmental Prediction/U. S. Department of Energy Global Reanalysis 2 (NCEP/DOE R2; Kanamitsu et al., 2002). The NCEP/DOE R2 data, which covers the period from 1979 to the present, has a horizontal resolution of 2.5° × 2.5° with 17 pressure levels from 1,000 to 10 hPa. Lastly, in order to obtain monthly means of the thermocline depth (defined as the depth of the 20°C isotherm) over the tropical Pacific, the Simple Ocean Data Assimilation product, version 2.2.4 (SODAv2.2.4; Carton & Giese, 2008) was utilized. The SODAv2.2.4 data, starting in 1871, has a horizontal resolution of 0.5° × 0.5° with 40 vertical levels from 5.01 to 5,375.0 m. For the purposes of model evaluation, we analyzed data for the period January 1982 to December 2011. Anomalies were defined as departures from the climatological seasonal cycle over the analysis period.

In this study, we analyze hindcast outputs produced by the Taiwan Central Weather Bureau (CWB) Climate Forecast System (CFS) 1-tiered model. The CWB model is a coupled atmosphere–ocean model that consists of the Central Weather Bureau Global Forecast System as its atmospheric model component (Saha et al., 2014; Xue et al., 2013) and the third version of Modular Ocean Model version as its oceanic model component (Pacanowski & Griffies, 1998). The CWB model has been shown to have reasonable skill in sub-seasonal to seasonal forecasts (cf. T. Y. Wu, Juang, et al., 2019) and is broadly used for evaluating the observed ENSO properties and global climate impacts (e.g., Chen et al., 2021a; Paek et al., 2015; J. W. Kim et al., 2021). The model hindcasts have a 1.0° × 1.0° horizontal resolution and cover the period from January 1982 to December 2011. For each month, hindcasts were launched at days 1, 3, 6, 8, 11, 13, 16, 18, 21, and 23, resulting in 10-member ensembles for each hindcast. The lead-0 to lead-8 months hindcasts analyzed were obtained as the monthly averages of these daily predictions (i.e., the 10-member ensembles). Thus, we have model hindcasts with lead times from 0 to 8 months for the period January 1982 to December 2011. Similar to the observational analysis, anomalies used were defined as departures from the model climatological seasonal cycle. For comparison, the hindcasted atmospheric variables, such as P_s, U, and V, were interpolated into a 2.5° × 2.5° horizontal resolution of the NCEP/DOE R2 dataset.

To examine the spatial complexity of ENSO, we analyzed the three types of El Niños (the EP, CP-I, and CP-II El Niños) using the events identified in Chen et al. (2021a). During the analysis period of 1982–2011, there were two extreme EP El Niños in 1982/83 and 1997/98, three CP-I El Niños in 1987/88, 1990/91, and 2002/03, and four CP-II El Niños in 1991/92, 1992/93, 2004/05, and 2009/10. This study does not include another well-known extreme El Niño event in 2015/16 in the analysis due to the limited model hindcast period and its unique and distinct characteristics compared to the previous two EP El Niño events in 1982/83 and 1997/98. Several recent studies have noted that the 2015/16 El Niño event cannot be clearly identified as an EP or CP type, as its warm SST anomalies shifted massively to the west, creating record-breaking warm anomalies over the tropical central Pacific. This is different from the 1982/83 and 1997/98 events, where warm SST anomalies during their peaks were mostly located in the tropical eastern equatorial Pacific (Paek et al., 2017; Santoso et al., 2017). Additionally, the 2015/16 El Niño exhibited distinctive evolution characteristics, as it was preceded by a weak El Niño event during 2014, while the 1982/83 and 1997/98 events were both preceded by opposite La Niña conditions (Kim & Yu, 2020).

To mitigate the small sample size of observed ENSO events, we conducted a significance test called the bootstrap test (Mudelsee, 2010). This bootstrap test enables us to assess the significance of the observational composites for the three types of El Niño despite their small sample sizes. Specifically, for the EP El Niño composite, we randomly selected 2 out of all 18 El Niño events during the period 1950–2020 (years provided by Chen et al., 2021a) and computed the composite of each random 2-event subset. We then repeated the procedure 1,000 times (to obtain 1,000 samples). Using these 1,000 random composites, we determined the range of one standard deviation that can be used as a statistical significance level for each of the El Niño composites. For the CP-I and CP-II El Niños, we randomly selected 3 and 4 events for the bootstrap composites, respectively. As shown in Figure 1, the bootstrap tests lend support to robustness of the observational composites discussed in the Introduction as they retain the distinct spatiotemporal characteristics of the observed EP, CP-I, and CP-II El Niño events. To examine the temporal complexity of ENSO, we specifically focus on the hindcasts of the multi-year evolution events during 1982–2011: the multi-year El Niño of 1986–1988 (namely, the 1986/87/88 El Niño) and the multi-year La Niña of 1998–2000 (namely, the 1998/99/00 La Niña). The calendar months of the year when an ENSO event develops (the first year) were denoted as January^0, February^0, …, and December^0. The calendar

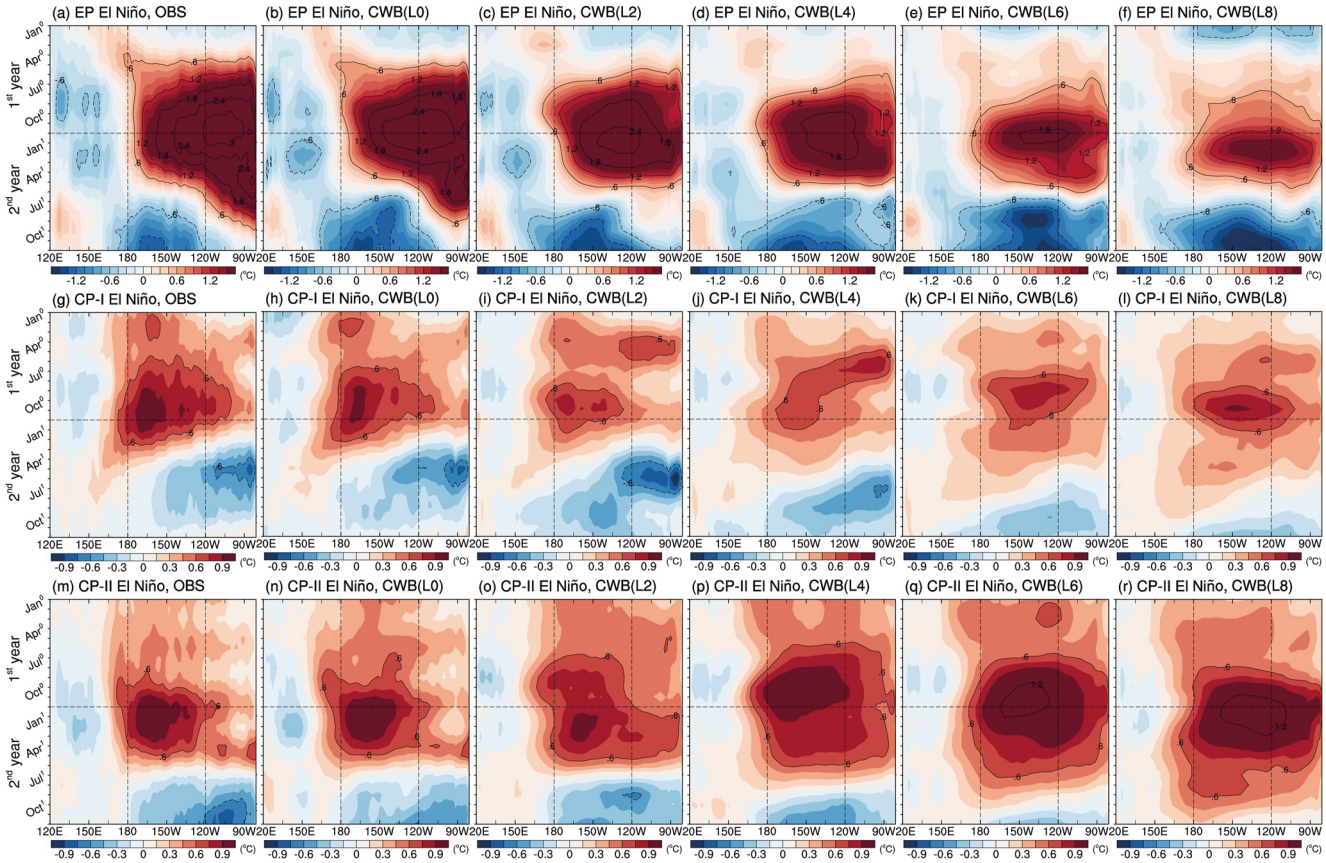

Figure 3. Longitude-time plots of equatorially-averaged (5°S−5°N) SST anomalies (in °C) for the EP El Niño during its developing (first year) and decaying (second year) years from (a) observations and (b–f) the CWB model hindcasts at lead times of 0, 2, 4, 6, and 8 months. (g–l) and (m–r) are the same as in (a–f), but for the CP-I El Niño and CP-II El Niño, respectively.

months of the year following an ENSO event (the second year) were denoted as January[1], February[1], …, and December[1], and so on for each subsequent year (the third year). All references to seasons in this study correspond to the Northern Hemisphere seasons.

3. Results

3.1. ENSO Complexity in Spatial Structure: The Three Types of El Niño

Figure 3 shows the longitude-time evolutions of equatorial Pacific SST anomalies during the three types of El Niño in the observations and the model hindcasts at various lead times. In the observations, the EP El Niño (Figure 3a) has warm SST anomalies originating off the South American coast during spring of the first year that extend westward during the summer and fall, reaching their maximum values during the winter, and then retreating toward back the coast during the spring and summer of the second year. It is also noticeable that the largest EP El Niño SST anomalies are mostly confined to the tropical eastern Pacific. In contrast, for the observed CP-I and CP-II El Niños (Figures 3g and 3m), the largest SST anomalies are concentrated in the tropical central Pacific and only very weak warm SST anomalies are found in the tropical eastern Pacific.

The hindcast results for the model accurately reproduce the observed longitude-time evolution features of the three types of El Niño at lead-0 (Figures 3b–3n), as expected. However, as the lead time increases, the hindcasts begin to diverge from the observations. In particular, when the lead month increases from lead-2 to lead-8, the hindcasts for EP El Niño consistently underestimate its intensity. This underestimation is most pronounced in the eastern and far-eastern tropical Pacific regions, leading to a shorter duration of El Niño conditions in those areas. Consequently, the hindcasted EP El Niño exhibits a faster termination and phase transition to La Niña during the decaying year, with the model error becoming more pronounced as the lead time increases. This deficiency of the

21698996, 2023, 14, Downloaded from https://agupubs.onlinelibrary.wiley.com/doi/10.1029/2022JD038200 by University Of California - Irvine, Wiley Online Library on [21/08/2023]. See the Terms and Conditions (https://onlinelibrary.wiley.com/terms-and-conditions) on Wiley Online Library for rules of use; OA articles are governed by the applicable Creative Commons License

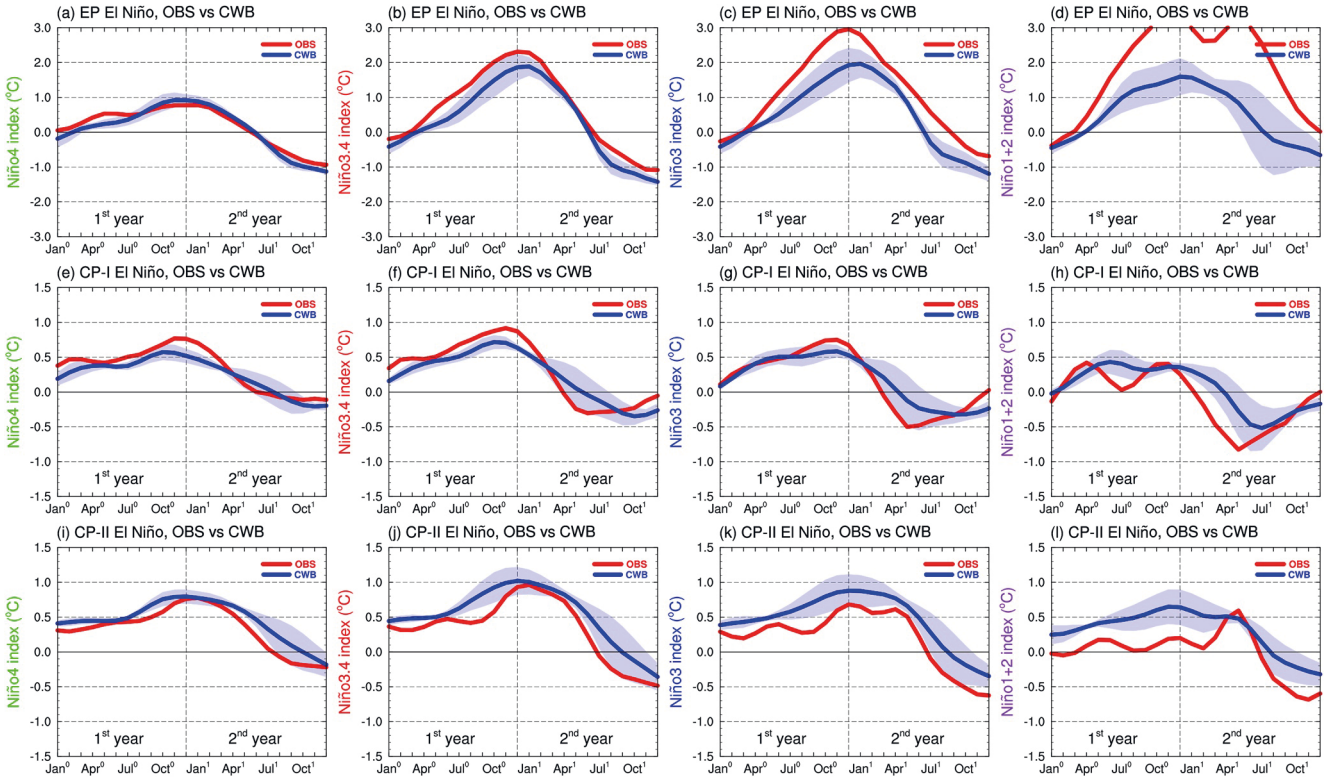

Figure 4. Temporal evolutions of the (a) Niño4, (b) Niño3.4, (c) Niño3, and (d) Niño1+2 indices (in °C) during the developing (first year) and decaying (second year) years for the EP El Niño in the observations (OBS; red curve) and the CWB model averaged over the lead-0 to lead-8 months hindcasts (blue curve) with the one standard deviation limits shown by the blue shading. (e–h) and (i–l) are the same as in (a–d), but for the CP-I El Niño and CP-II El Niño, respectively.

model is also evident in Figure 4, where we compare the temporal evolutions of the observed and hindcasted Niño indices (specifically, the rectangular regions in Figure 1a). Throughout the EP El Niño events (Figures 4a–4d), it is clear that the hindcasted Niño indices are consistently smaller than the observed ones during both the developing and decaying years. It should be noted that the hindcasted Niño indices shown in Figure 4 represent the mean index values averaged for the lead-0 to lead-8 months hindcasts, with the blue shadings denoting their one standard deviation ranges. The underestimation in the EP El Niño hindcasts is more severe for the Niño indices covering larger portions of the tropical eastern and far-eastern Pacific. Further statistical evidence supporting the significant underestimation of EP El Niño intensity by the model hindcasts during both the developing and decaying years can be found in Table 1. The table quantifies and compares El Niño intensities for the observations and model hindcasts, revealing substantial underestimation values such as −45.4% for the Niño3 index during the developing year and −71.1% for the Niño3 index during the decaying year.

For both the CP-I and CP-II El Niños, their longitude-time evolutions (Figures 3h–3l and 3n–3r) show that the model hindcasts generally reproduce the major features of the two CP El Niño types for all lead times. Despite this, some minor deficiencies exist. First, the model hindcasts tend to slightly underestimate (overestimate) El Niño intensity during the CP-I (CP-II) El Niño, particularly during its development and mature stages. A table comparing the various Niño index values averaged over the second half of the first year (i.e., July^0 to December^0) when the CP type El Niño typically develops and matures also captures this model deficiency as it shows negative (positive) percentages during the CP-I (CP-II) El Niño (see also Table 1). Secondly, the model hindcasts CP-I and CP-II El Niños tend to decay slower than the observed, causing their phase transition to be delayed by 2–3 months. These minor model deficiencies for the CP-I and CP-II El Niño hindcasts are also clearly seen in the temporal evolutions of the various Niño indices (Figure 4e–4l).

The results above indicate that the model has a noticeable deficiency in the hindcasts of the EP El Niño as it substantially underestimates El Niño intensity during both the developing and decaying years. Meanwhile, in spite of some minor deficiencies, the model is able to realistically hindcast the observed spatiotemporal evolutions of

21698996, 2023, 14, Downloaded from https://agupubs.onlinelibrary.wiley.com/doi/10.1029/2022JD038200 by University Of California - Irvine, Wiley Online Library on [21/08/2023]. See the Terms and Conditions (https://onlinelibrary.wiley.com/terms-and-conditions) on Wiley Online Library for rules of use; OA articles are governed by the applicable Creative Commons License

21698996, 2023, 14, Downloaded from https://agupubs.onlinelibrary.wiley.com/doi/10.1029/2022JD038200 by University Of California - Irvine, Wiley Online Library on [21/08/2023]. See the Terms and Conditions (https://onlinelibrary.wiley.com/terms-and-conditions) on Wiley Online Library for rules of use; OA articles are governed by the applicable Creative Commons License

Table 1
Mean Values of Four Different Niño Indices (in °C) for the Three Types of El Niño in the Observations (OBS) and the CWB Model Averaged Over All Lead-0 to Lead-8 Months Hindcasts and Their Differences in Percent (Relative to the Observations; Denoted as "Diff.")

EP El Niño	Niño4 index	Niño3.4 index	Niño3 index	Niño1+2 index
OBS	0.49 (−0.15)	1.04 (0.30)	1.32 (0.86)	1.64 (2.00)
CWB	0.40 (−0.18)	0.65 (0.02	0.72 (0.25)	0.67 (0.38)
Diff.	−17.6% (22.4%)	−38.2% (−97.7%)	−45.4% (−71.1%)	−59.3% (−81.2%)
CP-I El Niño	**Niño4 index**	**Niño3.4 index**	**Niño3 index**	**Niño1+2 index**
OBS	0.64	0.82	0.66	0.24
CWB	0.50	0.64	0.54	0.35
Diff.	−22.7%	−22.3%	−17.7%	44.4%
CP-II El Niño	**Niño4 index**	**Niño3.4 index**	**Niño3 index**	**Niño1+2 index**
OBS	0.57	0.60	0.43	0.10
CWB	0.68	0.86	0.75	0.56
Diff.	19.6%	42.1%	72.4%	438.1%

Note. Mean values were computed during the developing (first year) and decaying (second year; values in parentheses) years for the EP type while those were computed during the second half of the first year (July^0 to December^0) for the CP-I and CP-II types (see Text).

CP-I and CP-II El Niños with a lead time of up to eight (8) months. To further examine how model error grows in the hindcasts, we compare in Figures 5a–5c the hindcast and observed Niño3.4 index values for the three types of El Niño. It is evident from the figure that, as the lead time increases, the hindcast evolution of the index begins to deviate from the observed evolution for all three types of El Niño. However, when taking a closer look, the overall deviations are seen to be smallest for the CP-I El Niño, largest for the EP El Niño, and in-between for the CP-II El Niño. This result suggests that, for this particular model, the CP-I El Niño is the easiest El Niño type to be hindcast, followed by the CP-II El Niño, while the EP El Niño is the most difficult type to be hindcast. We then compute the growth of these hindcast errors by integrating the deviations between the hindcast and observed Niño3.4 index values over the El Niño lifecycle for each lead time. The integrated deviations can be expressed as follows:

$$\int |\bullet\ \ddot{\bullet}\bullet\bullet.\bullet.\ldots\bullet\bullet\bullet\ \bullet\ \ddot{\bullet}\bullet\bullet.\bullet\ldots\bullet\bullet\bullet| dt.$$

The bar-charts in Figures 5d–5f, which display the error growth in the hindcasts of the three types of El Niño, confirm the previous suggestion that the EP El Niño has the largest hindcast errors while the CP-II El Niño has the second largest and the CP-I El Niño has the smallest. It is also found from Figures 5d–5f that the hindcast errors for the EP and CP-II El Niños grow continually as the lead month increases, with the former growing relatively faster than the latter after 3-month lead. On the other hand, the hindcast errors for the CP-I El Niño grow very slowly and reach a plateau at the 8-month lead. Collectively, it can thus be concluded that the model has the best performance when hindcasting the CP-I El Niño, the second-best performance for the CP-II El Niño, and the worst performance for the EP El Niño.

There are a few issues that need to be addressed in depth when we separate the El Niño life cycle into the developing (first year) and decaying (second year) years, as shown in Figures 5g–5l. First, the errors in the simulation of the EP El Niño are quite bigger during its developing year than during its decaying year. The hindcast error grows rapidly as lead month increases during the developing year (Figure 5g) but maintains about the same magnitude during the decaying year (Figure 5j). This difference in error growth between the developing and decaying years may imply that the model is less capable of simulating the positive Bjerknes feedback processes (Bjerknes, 1969) crucial for the development of the EP El Niño but more capable of simulating the negative oceanic discharge and thermal damping processes (Wyrtki, 1985) crucial to the decay of the El Niño. In contrast, the hindcasts of the two CP type El Niños generally have smaller discrepancies (except for the decaying year of CP-II El Niño; Figures 5h and 5i vs. 5k, 5l). This diverse model performance supports the suggestion (cf. Yu, 2015; Yu

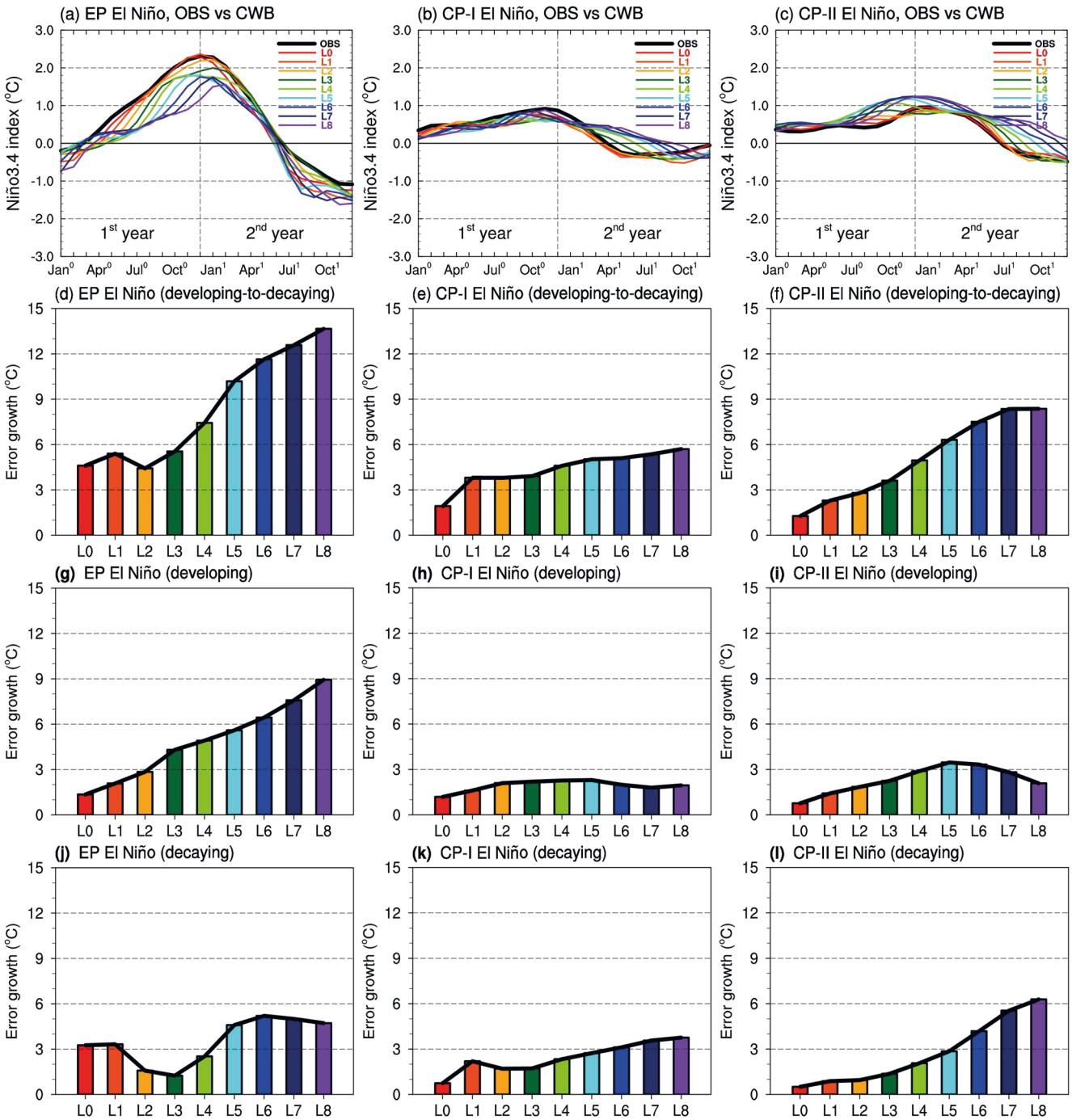

Figure 5. Temporal evolutions of the Niño3.4 index (in °C) in the observations (OBS; thick black curve) and the CWB model hindcasts at the lead-0 to lead-8 months lead times (L0 to L8; thin colored curves) for the (a) EP El Niño, (b) CP-I El Niño, and (c) CP-II El Niño during their developing (first year) and decaying (second year) years. (d–f) Bar-charts representing the error growth (in °C) calculated by integrating absolute differences in the Niño3.4 index between the CWB model hindcasts (from L0 to L8) and the OBS during the developing and decaying years for the (d) EP El Niño, (e) CP-I El Niño, and (f) CP-II El Niño. (g–i) and (j–l) are the same as (d–f) except during the developing year and the decaying year, respectively (see Text).

et al., 2017) that the dynamics of the CP El Niño primarily involves two-way interactions between the atmosphere and the ocean mixed layer in the tropical central Pacific (up to ~75 m). These interactions are less complicated than the EP El Niño dynamics that involve three-way interactions between the atmosphere, surface (~5 m), and subsurface (up to ~300 m) ocean layers in the tropical eastern Pacific. Consequently, the model hindcasts tend to exhibit smaller error growth for the two CP types of El Niño than for the EP type of El Niño. Furthermore, since

21698996, 2023, 14, Downloaded from https://agupubs.onlinelibrary.wiley.com/doi/10.1029/2022JD038200 by University Of California - Irvine, Wiley Online Library on [21/08/2023]. See the Terms and Conditions (https://onlinelibrary.wiley.com/terms-and-conditions) on Wiley Online Library for rules of use; OA articles are governed by the applicable Creative Commons License

21698996, 2023, 14, Downloaded from https://agupubs.onlinelibrary.wiley.com/doi/10.1029/2022JD038200 by University Of California - Irvine, Wiley Online Library on [21/08/2023]. See the Terms and Conditions (https://onlinelibrary.wiley.com/terms-and-conditions) on Wiley Online Library for rules of use; OA articles are governed by the applicable Creative Commons License

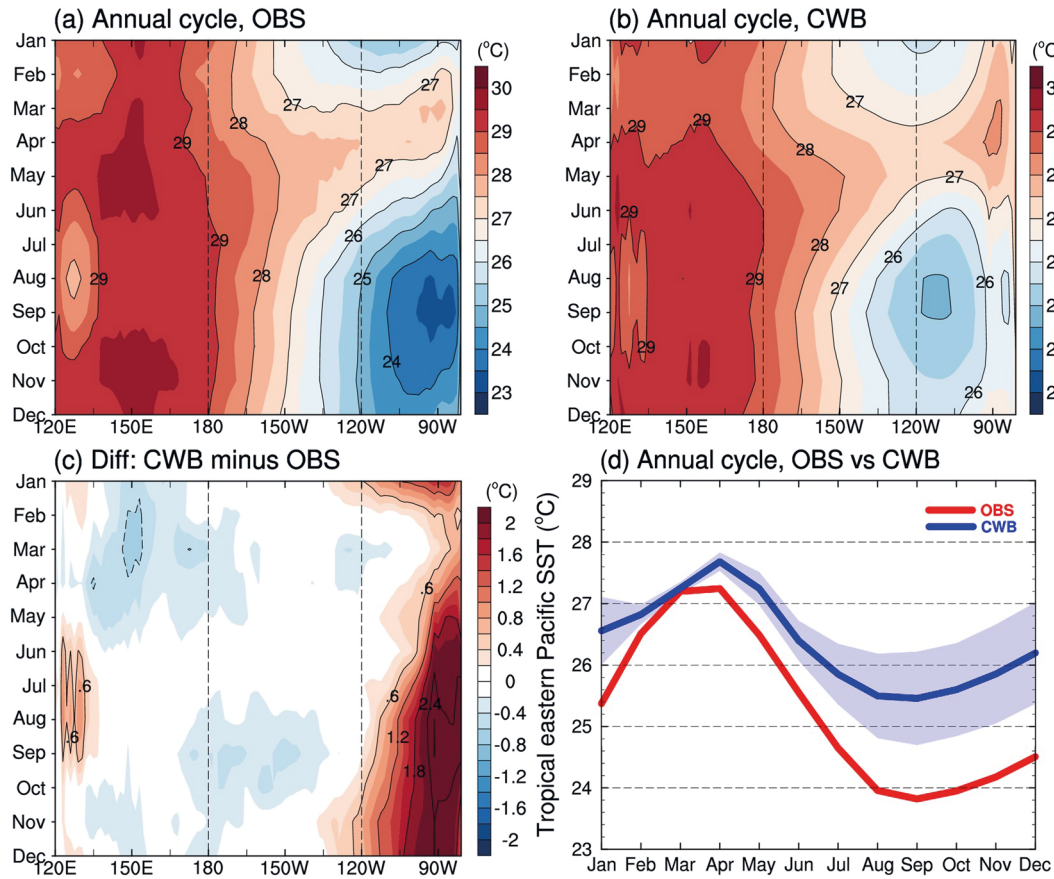

Figure 6. Annual cycles in the equatorially-averaged (i.e., 5°S−5°N) climatological SSTs (in °C) as a function of longitude for (a) the observations (OBS), (b) the CWB model averaged over the lead-0 to lead-8 months hindcasts, and (c) their difference (i.e., CWB minus OBS). (d) The annual cycle of climatological SSTs averaged over the tropical eastern Pacific (i.e., 5°S−5°N and 120−80°W) for the OBS (red curve) and the CWB model averaged over lead-0 to lead-8 months hindcasts (blue curve) with the one standard deviation limits shown by the blue shading.

the CP-II El Niño involves not only atmosphere-ocean mixed layer interactions *locally* over the tropical central Pacific but also *remotely* over the subtropical North Pacific regions (Chen et al., 2021a), the model tends to have larger errors in hindcasting the CP-II El Niño than in hindcasting the CP-I El Niño (which only involves the local atmosphere-ocean mixed layer interactions in the tropical central Pacific). The wind burst/disturbance, which is a stochastic white noise process that is less predictable, can also create an asymmetry in ENSO predictability between developing and decaying years. This is because it plays a more crucial role during the ENSO development phase than during the decay phase (Zheng et al., 2016).

What is responsible for the model's worse performance in hindcasts of the EP El Niño? The annual cycle plots of tropical Pacific climatological SSTs in the observations (Figure 6a) and the model hindcast mean (averaged from lead-0 to lead-8 months; Figure 6b) give us a clue. Compared to the observations (Figure 6a), it is seen that the model substantially overestimates the climatological SSTs in the tropical eastern Pacific, particularly to the east of 120°W (Figure 6b). This warm bias in the model is clearly revealed in the difference between the hindcast and observed climatological SSTs (Figure 6c). It is also evident in the annual cycles of the tropical eastern Pacific climatological SSTs (Figure 6d) that the warm bias tends to be stronger during the second half of the calendar year (July to December) than the first half (January to June). It can be suggested that this warm bias in the model simulates mean thermocline in the tropical eastern Pacific that is too deep. Figure 7, which presents the climatological thermocline depths in the tropical Pacific Ocean during fall (August to October, when the warm bias is largest) in the observations, the model hindcasts, and their difference, supports this suggestion by showing that the model in general has a deeper mean thermocline depth in the tropical eastern Pacific than observed. Note that the thermocline depth in the model hindcasts was obtained after removing biases by assuming that

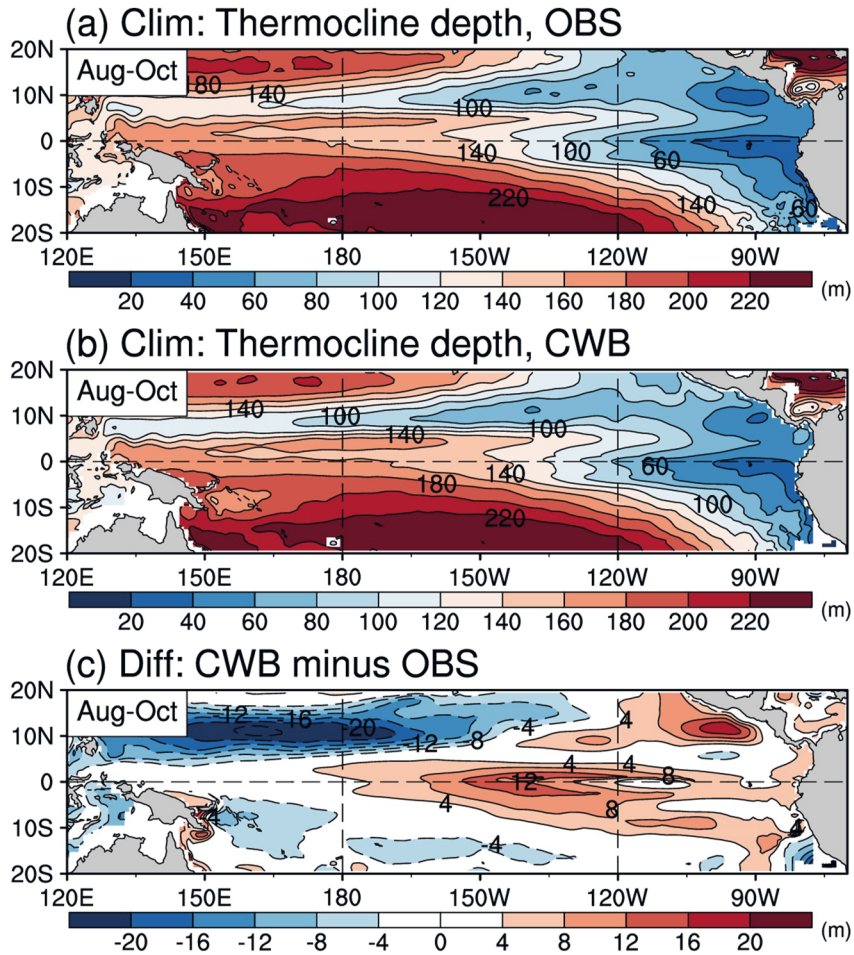

Figure 7. Climatological thermocline depth (20°C isotherm depth, in m) in the tropical Pacific Ocean basin during fall (August–October) for (a) the observations (OBS), (b) the CWB model averaged over lead-0 to lead-8 months hindcasts, and (c) their difference (i.e., CWB minus OBS).

the thermocline depth at lead-0 was the same as the observed (biases are inevitable due to the different vertical resolutions in the observational data and the model hindcast output). This model's deeper mean thermocline in the tropical eastern Pacific weakens the sensitivity of the overlying SSTs to wind variations due to a weakening of the so-called thermocline feedback in that region (An & Jin, 2001). When the mean thermocline is deeper (as in the model hindcasts), the strength of the surface wind stress-forced ocean wave that induces thermocline variations will also become weaker (An & Kim, 2017). It is well known that the SSTs in the tropical eastern Pacific are primarily influenced by subsurface ocean dynamics related to thermocline variations and their interactions with surface winds (i.e., the three-way interactions among the atmosphere, surface ocean, and subsurface ocean). As a consequence of these processes, the model tends to substantially underestimate El Niño intensity in the tropical eastern Pacific (Figures 3 and 4) and have worse hindcast performance for the EP El Niño (Figure 5). As we previously mentioned, the fundamental differences in ENSO dynamics between CP and EP El Niños (two-way vs. three-way interactions) could make it easier for the coupled model to hindcast CP El Niño compared to EP El Niño. Specifically, the CP-I type is the easiest to hindcast, followed by the CP-II type, and the EP type is the most difficult (as shown in Figures 3–5).

Next, we attempt to understand why the model hindcasts have this deficiency in simulating climatological SSTs and thermocline depths in the tropical eastern Pacific. Climatologically, the tropical Pacific Ocean exhibits a zonal contrast in SSTs between the western Pacific warm pool and the eastern Pacific cold tongue. Overly cold "cold tongue" SST can be established for at least two reasons. One is related to the strength of the Pacific Walker circulation, whose surface easterly winds cause the surface cooling in the cold tongue region via upwelling of

21698996, 2023, 14, Downloaded from https://agupubs.onlinelibrary.wiley.com/doi/10.1029/2022JD038200 by University Of California - Irvine, Wiley Online Library on [21/08/2023]. See the Terms and Conditions (https://onlinelibrary.wiley.com/terms-and-conditions) on Wiley Online Library for rules of use; OA articles are governed by the applicable Creative Commons License

21698996, 2023, 14, Downloaded from https://agupubs.onlinelibrary.wiley.com/doi/10.1029/2022JD038200 by University Of California - Irvine, Wiley Online Library on [21/08/2023]. See the Terms and Conditions (https://onlinelibrary.wiley.com/terms-and-conditions) on Wiley Online Library for rules of use; OA articles are governed by the applicable Creative Commons License

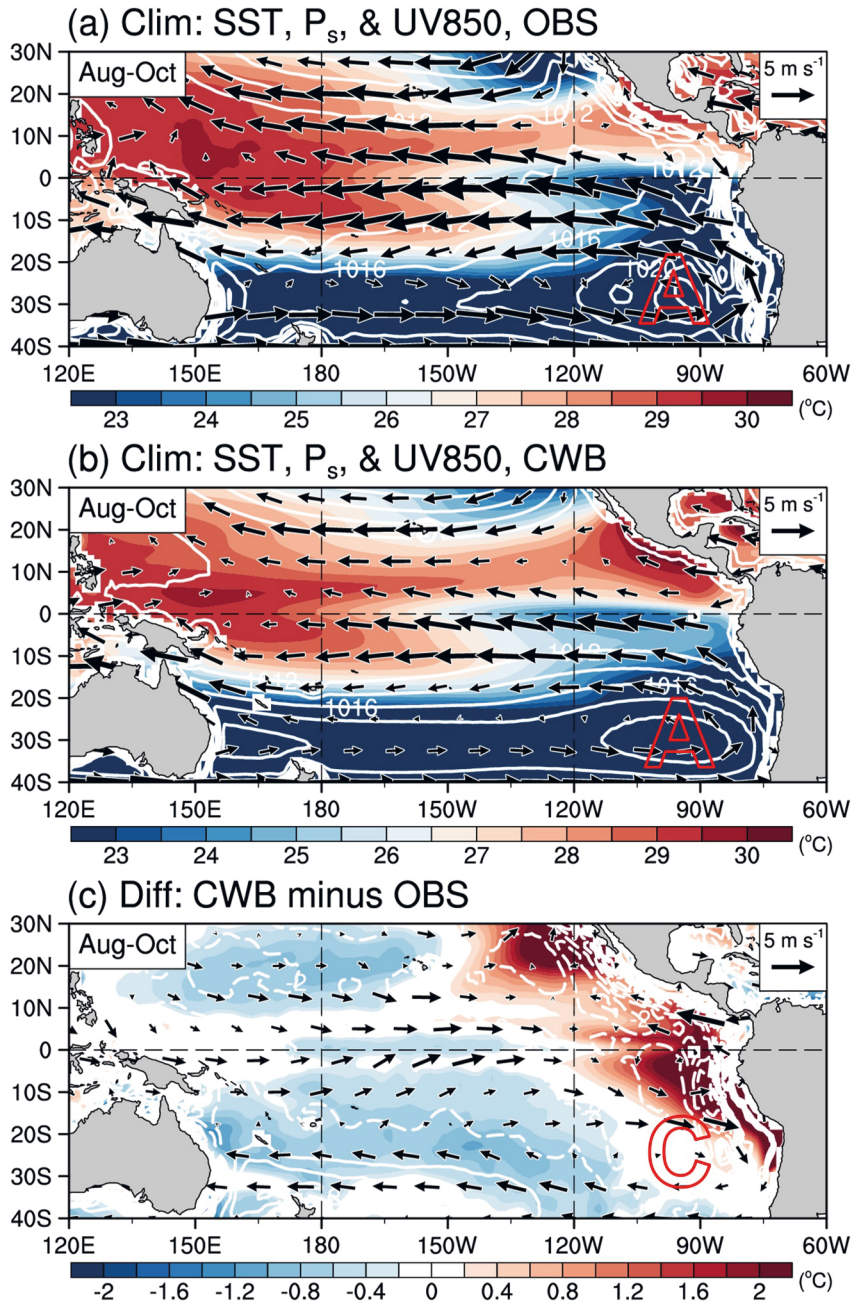

Figure 8. Climatological SSTs (shading; in °C), surface pressure (P_s; white contours; in hPa), and low-level winds at the 850-hPa level (UV850; vectors; in m s^{-1}) over the Pacific basin during fall (August–October) for (a) the observations (OBS), (b) the CWB model averaged over lead-0 to lead-8 months hindcasts, and (c) their difference (i.e., CWB minus OBS). The letter "A" denotes an anticyclonic circulation (which represents the location of the South Pacific high) while the letter "C" denotes a cyclonic circulation.

cold water from below. The other is related to the strength of the South Pacific high, a semi-permanent anti-cyclone located in the southeast Pacific near the west coast of Peru and northern Chile (see the letter "A" in Figures 8a and 8b), which can drive cross-equatorial surface winds in the tropical eastern Pacific that can also drive upwelling there. Figure 8a displays the observed climatological atmosphere and ocean structures over the Pacific basin during fall when the cold tongue SST are climatologically lowest. From the model hindcast mean (Figure 8b) and its difference from the observations (Figure 8c), it is evident that the simulated strengths of the Pacific Walker circulation and South Pacific high are weaker than in the observations. As shown in Figure 8c,

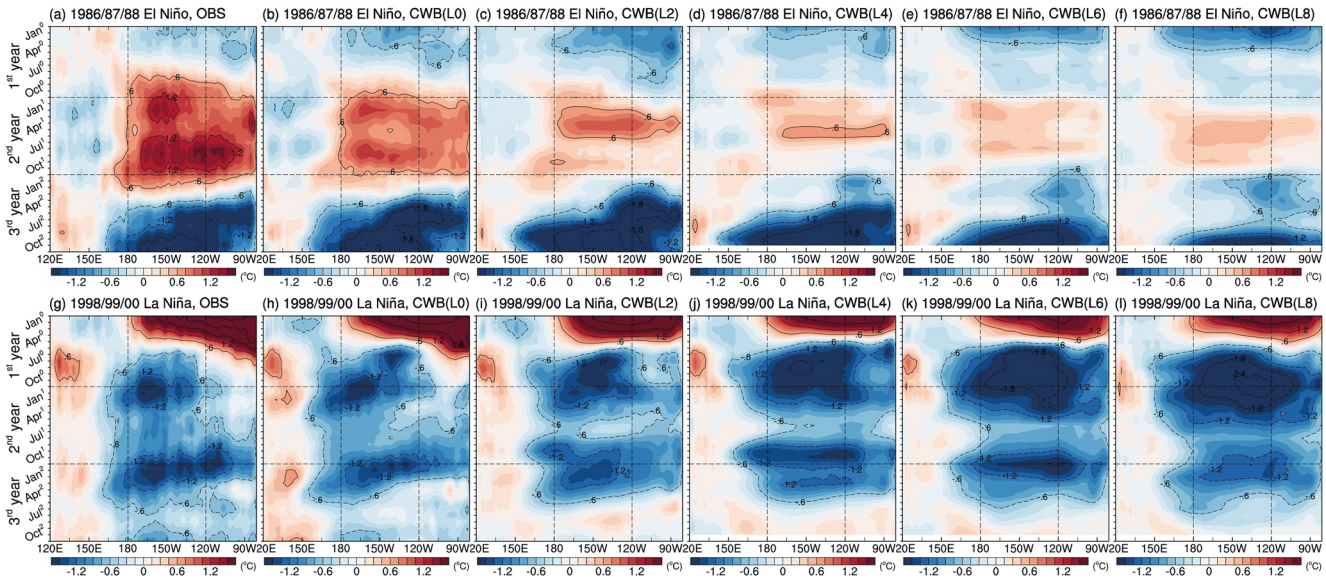

Figure 9. Longitude-time plots of equatorially-averaged (5°S−5°N) SST anomalies (in °C) during the 1986–88 El Niño from (a) the observations and (b–f) the CWB model hindcasts at lead 0, -2, -4, -6, and -8 months. (g–l) As in (a–f), but for the 1998–2000 La Niña.

the difference is characterized by surface westerlies along the equatorial Pacific (an indication of a weaker than observed Pacific Walker circulation) and a cyclonic circulation over the southeastern Pacific (an indication of a weaker than observed South Pacific high; see letter "C" in Figure 8c). These weaker-than-observed Pacific Walker circulation and South Pacific high in the model would each contribute to weaker than observed upwelling and thus warmer than observed cold tongue SSTs in the tropical eastern Pacific.

Further attributing these model deficiencies to a particular cause is difficult due to the strong coupling between atmosphere and ocean in the tropical eastern Pacific (Mechoso et al., 1995). Small model deficiencies in the atmospheric or oceanic model can be amplified by this coupling, thus easily affecting the coupled climate model performance. Previous studies have suggested that an inability to properly simulate the marine stratus clouds over the southeast Pacific in coupled models can influence the strength of the South Pacific high through radiative cooling (cf. Philander et al., 1996; Yu & Mechoso, 1999). A majority of contemporary climate models have difficulty properly simulating marine stratus clouds over the southeastern Pacific as well as the associated equatorial upwelling processes in the tropical Pacific (e.g., Gordon et al., 2000; Large & Danabasoglu, 2006).

3.2. ENSO Complexity in Temporal Evolution: The Multi-Year Evolution Events

To evaluate whether the model can or cannot correctly hindcast the observed temporal complexity of ENSO, as mentioned earlier, we focus on analyzing the multi-year ENSO events. Those are the multi-year El Niño which occurred in 1986–1988 (namely, the 1986/87/88 El Niño) and the multi-year La Niña which occurred in 1998–2000 (namely, the 1988/99/00 La Niña). Both are re-intensified ENSO events whose second-year peak intensity is larger than their first-year peak intensity (cf. Figure 2b). We first compare in Figure 8 the observed and hindcast longitude-time evolutions of equatorial Pacific SST anomalies. For the 1986/87/88 El Niño (Figure 9a), the warm SST anomalies emerge and develop mostly in the tropical central Pacific during the summer and fall of 1986 (the first year) and then peak during the following winter. While the El Niño persists into the spring of 1987 to start the second-year evolution, warm anomalies also emerge separately in the tropical eastern Pacific. The latter become dominant during the second-year of this event, when the largest warm anomalies are in the tropical eastern Pacific. This re-intensified multi-year El Niño can, therefore, be assumed to be a CP El Niño during its first-year and a mixture of CP/EP El Niño during its second-year. This SST evolution is similar to that observed during the 2014–2016 re-intensified multi-year El Niño (Kim & Yu, 2021; Paek et al., 2017). In the model hindcasts, despite a slight underestimate of El Niño intensity, the lead-0 months hindcast (Figure 9b) adequately reproduces the observed multi-year evolution of the 1986/87/88 event, capturing its first- and second-year peaks. However, as lead month increases from lead-2 to lead-8 (Figure 9c–9f), it is clear that the model fails to develop the

21698996, 2023, 14, Downloaded from https://agupubs.onlinelibrary.wiley.com/doi/10.1029/2022JD038200 by University Of California - Irvine, Wiley Online Library on [21/08/2023]. See the Terms and Conditions (https://onlinelibrary.wiley.com/terms-and-conditions) on Wiley Online Library for rules of use; OA articles are governed by the applicable Creative Commons License

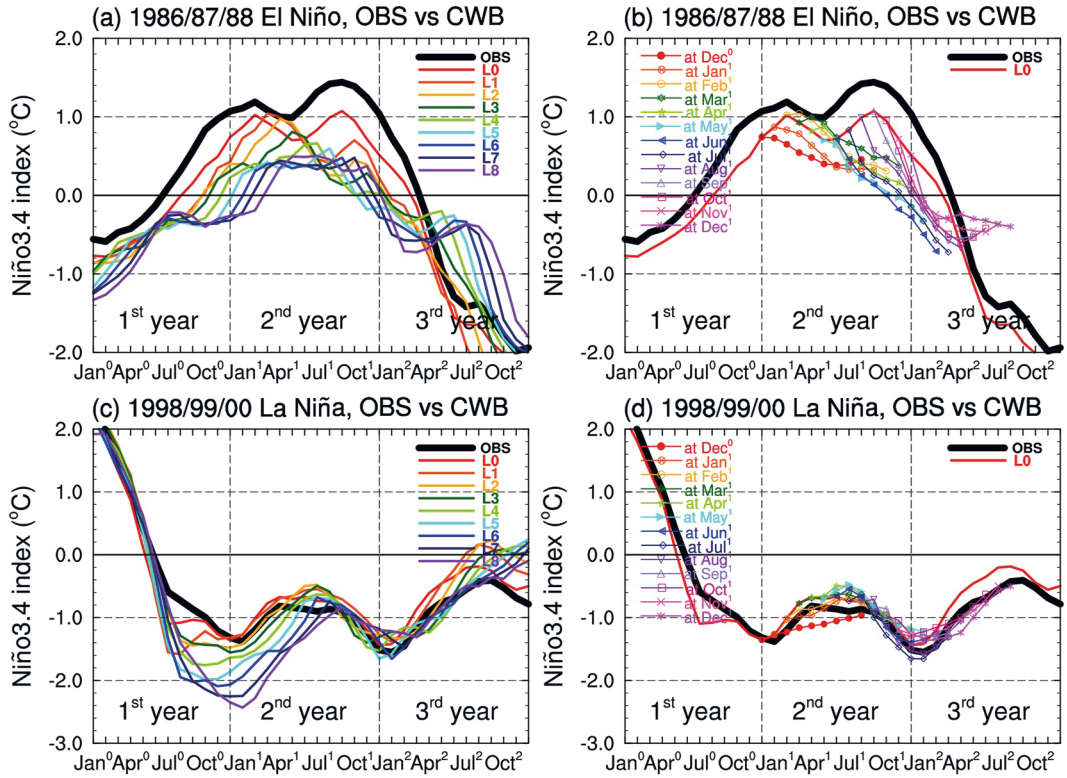

Figure 10. (a), (c) Temporal evolutions of the Niño3.4 index (°C) in the observations (OBS; thick black curve) and the CWB model hindcasts at the lead-0 to lead-8 months (L0 to L8; thin colored curves) for the (a) 1986–88 El Niño and (c) 1998–2000 La Niña. (b), (d) As in (a), (c) but using model hindcasts that are launched from different starting months from December^0 to December^1 (thin curves with various colors and markers). The red curve denotes the Niño3.4 index evolution in the lead-0 months hindcast.

second-year El Niño that occurs during 1987. The hindcast event, instead, tends to become a single-year El Niño with its peak in around the spring/summer of 1987 before transitioning into a La Niña afterward. Figure 10a, which displays the evolution of the observed and hindcast Niño3.4 indices also clearly shows this model failure.

We extend our analysis to evaluate whether the model hindcasts have an ability to forecast the multi-year El Niño of 1986–1988. To achieve this, we plot the same Niño3.4 index evolutions as in Figure 10a but using the individual model hindcasts that are launched at different starting months from December^0 to December^1 (Note. the lead-0 months hindcast values were utilized as initial conditions.). As depicted by thin curves with various colors and markers in Figure 10b, the results clearly indicate that the model is not capable of forecasting the 1986/87/88 El Niño's multi-year evolution. Once they are launched at any starting month, the initial Niño3.4 index values have an immediate downward slope toward a neutral or negative ENSO phase, failing to capture the re-intensification of the 1986/87/88 El Niño.

We next examine for this event the horizontal maps of seasonally-averaged SST and wind anomalies during the first-year winter, following spring, and summer to determine why the model hindcasts fail to capture the re-intensification of the 1986/87/88 El Niño. For the observations (Figure 11a–11c), it is clear that the El Niño, after initial first-year peak in winter, persists and re-intensifies during the following spring and summer to give rise to its second-year peak. Meanwhile, during the first-year winter (Figure 11a), we also see that there is a meridional band of warm SST anomalies extending from the subtropical northeastern Pacific to the tropical central Pacific that is accompanied by southwesterly wind anomalies in-between (see parallelograms in Figure 11). This meridional band of anomalous SST warming in the subtropical northeastern Pacific is also known as a positive PMM(Chiang & Vimont, 2004). The positive PMM, which is often induced by CP El Niño as a result of the El Niño's teleconnections to the extratropics (Fang & Yu, 2020b; Stuecker, 2018), is able to be sustained for several seasons and its warm anomalies spread into the equatorial Pacific via a wind–evaporation–SST feedback mechanism (Xie & Philander, 1994), enabling another El Niño to develop (Amaya, 2019; Kim

21698996, 2023, 14, Downloaded from https://agupubs.onlinelibrary.wiley.com/doi/10.1029/2022JD038200 by University Of California - Irvine, Wiley Online Library on [21/08/2023]. See the Terms and Conditions (https://onlinelibrary.wiley.com/terms-and-conditions) on Wiley Online Library for rules of use; OA articles are governed by the applicable Creative Commons License

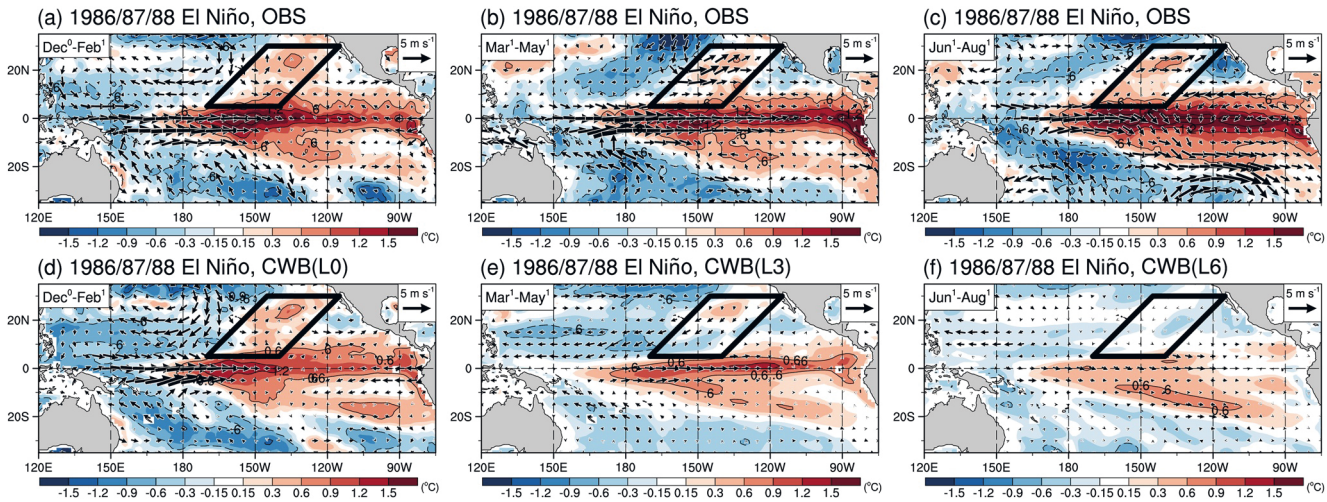

Figure 11. Seasonally-averaged anomalies in SST (shading; °C) and low-level winds at the 850-hPa level (vectors; m s^{-1}) for the 1986–88 El Niño during its (a) first-year winter (December^0–February^1), (b) following spring (March^1–May^1), and (c) summer (June^1–August^1) from the observations (OBS). (d–f) as in (a–c) but for the CWB model hindcasts at the lead times of (d) 0, (e) 3, and (f) 6 months. The subtropical northeastern Pacific region where the PMM events usually occur is delineated by the black parallelogram.

& Yu, 2020, 2021, 2022; Yu et al., 2010; Yu & Kim, 2011). As shown in Figure 11a–11c, the abovementioned tropical–subtropical climate interactions within the Pacific basin are at work during the re-intensification of the 1986/87/88 El Niño. Note that an EP El Niño is less likely to induce a positive PMM, making it less capable of activating the Pacific intrabasin interactions. In fact, Fang and Yu (2020b) found that that an EP El Niño is more likely to induce a negative PMM through a Gill-type response (Gill, 1980) in the tropical eastern Pacific, particularly when it has an extreme amplitude, such as during the 1982/83 and 1997/98 events. In contrast to the observations, in the model hindcasts (Figures 11d–11f) the positive PMM during the first-year winter (represented by the anomalous SST warming and southwesterly wind in the subtropical northeastern Pacific) suddenly disappears and is replaced by anomalous cooling and northeasterly wind anomalies during the following spring and summer. This indicates that the Pacific intrabasin interactions are not realistically simulated in the hindcasts and the hindcasts fail to forecast the re-intensification.

For the multi-year La Niña event of 1998–2000 (Figure 9g), we find that the hindcasts generally reproduce the multi-year evolution, not only for the lead-0 months hindcast (Figure 9h), but also for hindcasts at lead-2, 4, 6, and 8 months (Figures 9i–9l), although the intensity of the hindcast first-year La Niña is excessively strong as the lead month increases (Figure 10c). The evolution of the Niño3.4 index shown in Figures 10c and 10d confirms that all the individual model hindcasts successfully simulate the re-intensification evolution feature of the 1998/99/00 La Niña regardless of the launching month. Why, in stark contrast to the model's failure to forecast the 1986/87/88 El Niño evolution, is the model able to successfully forecast the 1998/99/00 La Niña evolution? We find in Figure 12, which uses the same horizontal maps as in Figure 11 but for the 1998/99/00 La Niña, that the model reproduces the observed Pacific intrabasin interactions in the La Niña hindcasts. During the first-year winter, following spring, and summer of the 1998/99/00 La Niña, the model hindcasts properly simulate the observed negative PMM with anomalous SST cooling and northeasterly winds in the subtropical northeastern Pacific (Figures 12a–12c vs. 12d–12f; see also parallelograms). This indicates that, contrary to the El Niño hindcasts, the model is able to capture the Pacific intrabasin interactions activated by the first-year La Niña during 1998–1999 to successfully forecast the re-intensification of the second-year La Niña during 1999–2000.

One question that still remains is: why can the La Niña event activate the Pacific intrabasin interactions in the model to produce the multi-year evolution pattern but the El Niño event cannot? In this regard, we find in Figures 13a and 13b that the simulated climatological SSTs in the tropical central Pacific are too cold compared to the observations during spring, which is the season when the PMM is most active (Chiang & Vimont, 2004). This cold bias provides more favorable conditions for La Niña to activate the Pacific intrabasin interactions but not for El Niño. This is because, as the cold bias lowers climatological SSTs closer to the convective threshold temperature (~28°C, Sud et al., 1999; see dark green contours in Figures 13a and 13b), the La Niña-related

21698996, 2023, 14, Downloaded from https://agupubs.onlinelibrary.wiley.com/doi/10.1029/2022JD038200 by University Of California - Irvine, Wiley Online Library on [21/08/2023]. See the Terms and Conditions (https://onlinelibrary.wiley.com/terms-and-conditions) on Wiley Online Library for rules of use; OA articles are governed by the applicable Creative Commons License

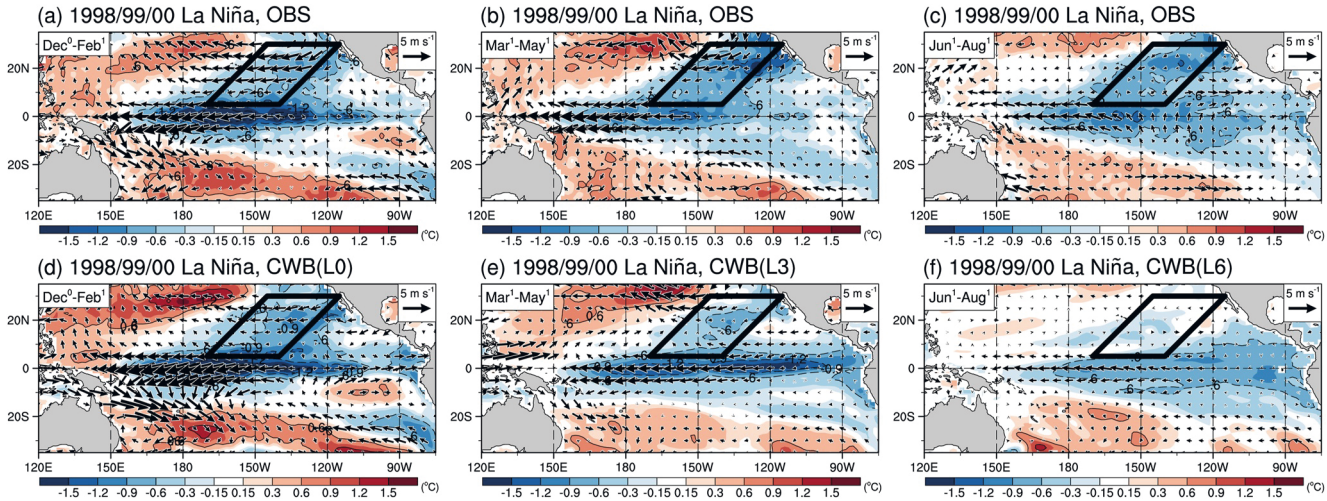

Figure 12. As in Figure 11 but for the 1998–2000 La Niña.

cold anomalies can easily bring down SSTs below the threshold value in the tropical central Pacific and switch off deep convection. The induced large anomalous cooling can then excite an anomalous anticyclone over the subtropical Pacific, including the PMM region, activating a negative phase of the Pacific intrabasin interactions, whose cold anomalies can later intrude into the equatorial Pacific to initiate the second-year La Niña. The bar-charts representing the climatological tropical central Pacific spring SSTs (black rectangles in Figures 13a and 13b) in the observations and the model hindcast (Figure 13c) confirm that the model's cold bias is statistically significant. Although the El Niño-related warm anomalies can strengthen deep convection over the tropical central Pacific to produce anomalous heating in that region, the heating is relatively small compared to the cooling induced by a La Niña event that completely turns off the climatological deep convection. Also, since most CP El Niño events have weak intensities (e.g., Kao & Yu, 2009; T. Lee & McPhaden, 2010), the anomalous heating they induce is weak and provides less favorable conditions for El Niño to activate the Pacific intrabasin interactions. The physical mechanism explaining the La Niña-favored activation of the Pacific intrabasin interactions has been well documented in Fang and Yu (2020b).

4. Summary and Discussion

In this study, we evaluated hindcasts of the observed spatiotemporal complexity in the ENSO during the period 1982−2011 made using the Taiwan Central Weather Bureau (CWB) Climate Forecast System (CFS) 1-tiered model hindcasts. The main findings of this study are summarized as follows. Concerning hindcasts of the spatial complexity, it is found that the CP-I El Niño is the easiest to hindcast for this particular climate model, followed by the CP-II El Niño, while the EP El Niño is the most difficult type. The model significantly underestimated the observed EP El Niño intensity during both the developing and decaying years, while the model slightly underestimated (overestimated) the CP-I (CP-II) El Niño intensity and produced a slower decay of these events. The model deficiency in the EP El Niño hindcasts was shown to be related to a warm bias in the model SST climatology in the tropical eastern Pacific. This warm bias is associated with a bias in thermocline depth that weakens the atmosphere–ocean coupling in the tropical eastern Pacific that reduces the intensity of hindcasted EP El Niños. The strengths of the Pacific Walker circulation and South Pacific high—both of which were weaker than observed—in the model climatology was identified as the cause of the model's warm bias in the tropical eastern Pacific.

Concerning the temporal complexity, it was found that the model is better able to hindcast multi-year La Niña than multi-year El Niño. The model deficiency in the multi-year El Niño hindcasts was found to be related to a cold bias in the model SST climatology in the tropical central Pacific. This cold bias causes the model to enable La Niña, but not El Niño, to activate intrabasin tropical–subtropical interactions associated with the PMM that produce the multi-year evolution pattern. It should be also noted that the model in general has a better hindcast performance for single-year ENSO events than multi-year ones, such as the single-year events of 1997/98 El Niño and 2005/06 La Niña (cf. Figure 2a) (figures not shown). This conclusion can also be supported by the fact

21698996, 2023, 14, Downloaded from https://agupubs.onlinelibrary.wiley.com/doi/10.1029/2022JD038200 by University Of California - Irvine, Wiley Online Library on [21/08/2023]. See the Terms and Conditions (https://onlinelibrary.wiley.com/terms-and-conditions) on Wiley Online Library for rules of use; OA articles are governed by the applicable Creative Commons License

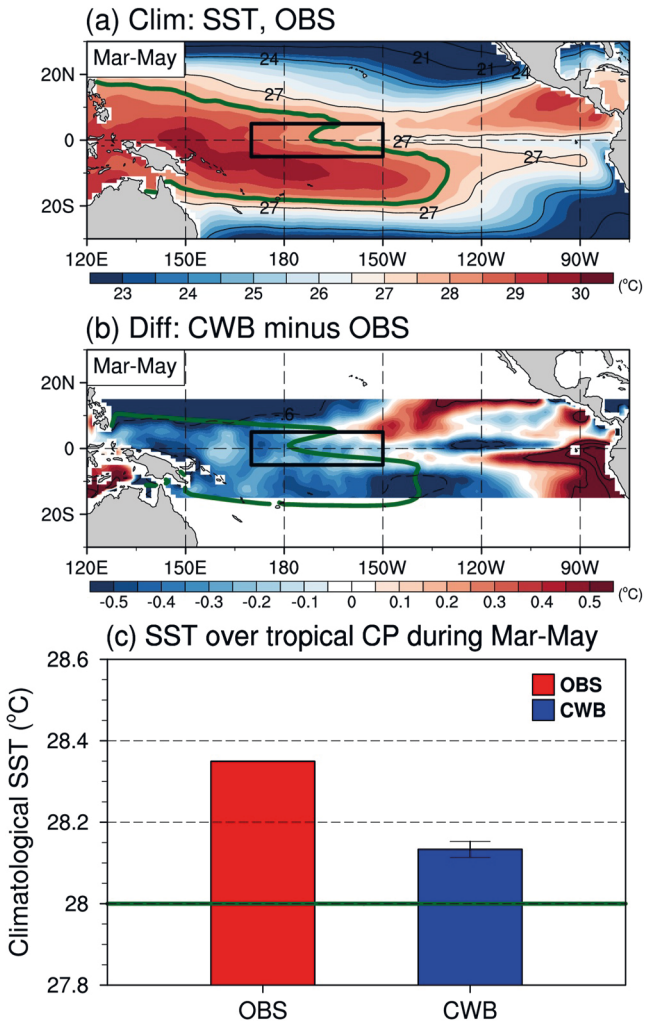

Figure 13. Climatological SSTs (°C) during spring (March−May) for (a) the observations (OBS) and (b) its difference within the tropical band between 15°S and 15°N from the CWB model averaged over the lead-0 to lead-8 months hindcasts (i.e., CWB minus OBS). The dark green contours in (a) and (b) denote the 28°C isotherm which indicates the threshold SST value for deep convection in the OBS and CWB model, respectively. The black rectangles indicate the selected tropical central Pacific region bounded by 5°S−5°N, 170°E−150°W. (c) Bar-chart representing climatological SSTs averaged over the tropical central Pacific for the OBS (red bar) and the CWB model hindcasts (blue bar). In (c), the error bar denotes one standard deviation among all the lead months from lead-0 to lead-8 and the dark green horizontal line indicates the 28°C threshold SST.

that many contemporary climate models, despite progress in simulating basic ENSO features, are still struggling with the tendency to produce a sharp, biennial ENSO oscillation rather than a broad spectral peak in the 3−7-year band (e.g., Bellenger et al., 2014; Guilyardi et al., 2009; Jha et al., 2014). Therefore, an improved representation of the observed ENSO's major frequencies within climate models may provide enhanced ENSO predictability and improve forecasts of multi-year events. It was also shown in Figures 4 and 5 that El Niño is generally more predictable during its decay phase than its growth phase for the EP type (see also Zheng et al., 2016), while the opposite seems to be true for the CP type (including CP-I and CP-II El Niños). This contrasting predictability between EP and CP type El Niños deserves further investigations in future studies, including the potential role of weather noise in influencing the spatiotemporal complexity of ENSO (e.g., J. W. Lee et al., 2019).

The number of observed El Niño events analyzed in this study is limited. This is a well-known challenge faced by most studies of ENSO complexity because the relatively small number of observed events must be separated into subgroups with different spatiotemporal characteristics. The ensemble hindcast approach presented in this study could be a useful way to study the predictability of the three types of El Niño given the limited availability of observational data. In this approach, each member of the ensemble is independently integrated forward for several months and seasons from the same initial atmospheric and oceanic conditions before the hindcasted results are examined. The mean features, which are averaged from the ensemble members, reflect the common properties of the simulated phenomenon (in this study, the EP, CP-I, and CP-II El Niños types) and the model's performance in hindcasting the target phenomenon.

Finally, we need to acknowledge that the main results of this study could be dependent on the model used. For instance, in contrast to our conclusion that the EP El Niño is the most difficult El Niño type to hindcast, some previous studies (e.g., Hu et al., 2012; Xue et al., 2013) have shown that hindcast simulations produced by NCEP's Climate Forecast System (CFS) models tend to have higher forecasting skill for EP El Niños than CP El Niños. This difference may be related to the different ENSO dynamics in the models. Additionally, Yu and Fang (2018) suggested that climate models dominated by the tropical Pacific ENSO dynamics produce different ENSO complexities from those dominated by the subtropical Pacific ENSO dynamics. Although we only used a specific model, this study provides a unique and significant advantage by offering physical processes to explain model discrepancies from observations regarding ENSO's spatiotemporal complexity, as described in Sections 3.1 (ENSO complexity in spatial structure) and 3.2 (ENSO complexity in temporal evolution). By presenting these processes, readers may gain valuable information and insights into the missing processes that account for discrepancies in their own climate models when simulating or hindcasting complex ENSO behaviors in observations.

Data Availability Statement

The resources of data used in this study are as follows. The HadISSTv1.1 data (Rayner et al., 2003) are available at https://www.metoffice.gov.uk/hadobs/. The NCEP/DOE R2 data (Kanamitsu et al., 2002) are available at https://www.esrl.noaa.gov/psd/data/gridded/data.ncep.reanalysis2.html. The SODAv2.2.4 data (Carton & Giese, 2008) are available at https://iridl.ldeo.columbia.edu/SOURCES/.CARTON-GIESE/.SODA/.v2p2p4/?Set-Language=en.

21698996, 2023, 14, Downloaded from https://agupubs.onlinelibrary.wiley.com/doi/10.1029/2022JD038200 by University Of California - Irvine, Wiley Online Library on [21/08/2023]. See the Terms and Conditions (https://onlinelibrary.wiley.com/terms-and-conditions) on Wiley Online Library for rules of use; OA articles are governed by the applicable Creative Commons License

Acknowledgments
The authors thank the editor Dr. Rong Fu and the three anonymous reviewers whose constructive comments and careful suggestions have greatly improved this study. The authors are also very thankful to all observational data providers. All of the datasets utilized in this study are accessible through the web links provided in the Open Research section (Data Availability Statement). This research was supported by a grant from the Central Weather Bureau of Taiwan under Grant IISI-202924. J.-W. Kim and J.-Y. Yu were also supported by NSF Climate and Large-Scale Dynamics Program under grants AGS-1833075 and 2109539.

References

Amaya, D. J. (2019). The Pacific meridional mode and ENSO: A review. *Current Climate Change Reports*, *5*(4), 296–307. https://doi.org/10.1007/s40641-019-00142-x

An, S. I., & Jin, F. F. (2001). Collective role of thermocline and zonal advective feedbacks in the ENSO mode. *Journal of Climate*, *14*(16), 3421–3432. https://doi.org/10.1175/1520-0442(2001)014<3421:crotaz>2.0.co;2

An, S. I., & Kim, J. W. (2017). Role of nonlinear ocean dynamic response to wind on the asymmetrical transition of El Niño and La Niña. *Geophysical Research Letters*, *44*(1), 393–400. https://doi.org/10.1002/2016gl071971

An, S. I., & Kim, J. W. (2018). ENSO transition asymmetry: Internal and external causes and intermodel diversity. *Geophysical Research Letters*, *45*(10), 5095–5104. https://doi.org/10.1029/2018gl078476

An, S. I., Tziperman, E., Okumura, Y. M., & Li, T. (2020). ENSO irregularity and asymmetry. *El Niño Southern Oscillation in a Changing Climate*, 153–172. https://doi.org/10.1002/9781119548164.ch7

Barnston, A. G., Tippett, M. K., Ranganathan, M., & L'Heureux, M. L. (2019). Deterministic skill of ENSO predictions from the North American multimodel ensemble. *Climate Dynamics*, *53*(12), 7215–7234. https://doi.org/10.1007/s00382-017-3603-3

Bellenger, H., Guilyardi, É., Leloup, J., Lengaigne, M., & Vialard, J. (2014). ENSO representation in climate models: From CMIP3 to CMIP5. *Climate Dynamics*, *42*(7), 1999–2018. https://doi.org/10.1007/s00382-013-1783-z

Bjerknes, J. (1969). Atmospheric teleconnections from the equatorial Pacific. *Monthly Weather Review*, *97*(3), 163–172. https://doi.org/10.1175/1520-0493(1969)097<0163:atftep>2.3.co;2

Capotondi, A., Wittenberg, A. T., Newman, M., Di Lorenzo, E., Yu, J. Y., Braconnot, P., et al. (2015). Understanding ENSO diversity. *Bulletin of the American Meteorological Society*, *96*(6), 921–938. https://doi.org/10.1175/bams-d-13-00117.1

Carton, J. A., & Giese, B. S. (2008). A reanalysis of ocean climate using simple ocean data assimilation (SODA). *Monthly Weather Review*, *136*(8), 2999–3017. https://doi.org/10.1175/2007mwr1978.1

Chen, M., Chang, T. H., Lee, C. T., Fang, S. W., & Yu, J. Y. (2021). A study of climate model responses of the Western Pacific subtropical high to El Niño diversity. *Climate Dynamics*, *56*(1), 581–595. https://doi.org/10.1007/s00382-020-05500-2

Chen, M., Yu, J. Y., Wang, X., & Chen, S. (2021). Distinct onset mechanisms of two subtypes of CP El Niño and their changes in future warming. *Geophysical Research Letters*, *48*(14), e2021GL093707. https://doi.org/10.1029/2021gl093707

Chen, M., Yu, J. Y., Wang, X., & Jiang, W. (2019). The changing impact mechanisms of a diverse El Niño on the Western Pacific subtropical high. *Geophysical Research Letters*, *46*(2), 953–962. https://doi.org/10.1029/2018gl081131

Chiang, J. C., & Vimont, D. J. (2004). Analogous Pacific and Atlantic meridional modes of tropical atmosphere–ocean variability. *Journal of Climate*, *17*(21), 4143–4158. https://doi.org/10.1175/jcli4953.1

Choi, K. Y., Vecchi, G. A., & Wittenberg, A. T. (2013). ENSO transition, duration, and amplitude asymmetries: Role of the nonlinear wind stress coupling in a conceptual model. *Journal of Climate*, *26*(23), 9462–9476. https://doi.org/10.1175/jcli-d-13-00045.1

DiNezio, P. N., & Deser, C. (2014). Nonlinear controls on the persistence of La Niña. *Journal of Climate*, *27*(19), 7335–7355. https://doi.org/10.1175/jcli-d-14-00033.1

Dommenget, D., Bayr, T., & Frauen, C. (2013). Analysis of the non-linearity in the pattern and time evolution of El Niño southern oscillation. *Climate Dynamics*, *40*(11), 2825–2847. https://doi.org/10.1007/s00382-012-1475-0

Fang, S. W., & Yu, J. Y. (2020a). Contrasting transition complexity between El Niño and La Niña: Observations and CMIP5/6 models. *Geophysical Research Letters*, *47*(16), e2020GL088926. https://doi.org/10.1029/2020gl088926

Fang, S. W., & Yu, J. Y. (2020b). A control of ENSO transition complexity by tropical Pacific mean SSTs through tropical-subtropical interaction. *Geophysical Research Letters*, *47*(12), e2020GL087933. https://doi.org/10.1029/2020gl087933

Gill, A. E. (1980). Some simple solutions for heat-induced tropical circulation. *Quarterly Journal of the Royal Meteorological Society*, *106*(449), 447–462. https://doi.org/10.1002/qj.49710644905

Gordon, C. T., Rosati, A., & Gudgel, R. (2000). Tropical sensitivity of a coupled model to specified ISCCP low clouds. *Journal of Climate*, *13*(13), 2239–2260. https://doi.org/10.1175/1520-0442(2000)013<2239:tsoacm>2.0.co;2

Guilyardi, E., Wittenberg, A., Fedorov, A., Collins, M., Wang, C., Capotondi, A., et al. (2009). Understanding El Niño in ocean–atmosphere general circulation models: Progress and challenges. *Bulletin of the American Meteorological Society*, *90*(3), 325–340. https://doi.org/10.1175/2008bams2387.1

Hu, Z. Z., Kumar, A., Jha, B., Wang, W., Huang, B., & Huang, B. (2012). An analysis of warm pool and cold tongue El Niños: Air–sea coupling processes, global influences, and recent trends. *Climate Dynamics*, *38*(9), 2017–2035. https://doi.org/10.1007/s00382-011-1224-9

Hu, Z. Z., Kumar, A., Xue, Y., & Jha, B. (2014). Why were some La Niñas followed by another La Niña? *Climate Dynamics*, *42*(3), 1029–1042. https://doi.org/10.1007/s00382-013-1917-3

Iwakiri, T., & Watanabe, M. (2020). Multiyear La Niña impact on summer temperature over Japan. *Journal of the Meteorological Society of Japan Series II*, *98*(6), 1245–1260. https://doi.org/10.2151/jmsj.2020-064

Jha, B., Hu, Z. Z., & Kumar, A. (2014). SST and ENSO variability and change simulated in historical experiments of CMIP5 models. *Climate Dynamics*, *42*(7), 2113–2124. https://doi.org/10.1007/s00382-013-1803-z

Kanamitsu, M., Ebisuzaki, W., Woollen, J., Yang, S. K., Hnilo, J. J., Fiorino, M., & Potter, G. L. (2002). Ncep–doe amip-ii reanalysis (r-2). *Bulletin of the American Meteorological Society*, *83*(11), 1631–1643. https://doi.org/10.1175/bams-83-11-1631(2002)083<1631:nar>2.3.co;2

Kao, H. Y., & Yu, J. Y. (2009). Contrasting eastern-Pacific and central-Pacific types of ENSO. *Journal of Climate*, *22*(3), 615–632. https://doi.org/10.1175/2008jcli2309.1

Kim, H. M., Webster, P. J., & Curry, J. A. (2009). Impact of shifting patterns of Pacific Ocean warming on North Atlantic tropical cyclones. *Science*, *325*(5936), 77–80. https://doi.org/10.1126/science.1174062

Kim, J. W., Chang, T. H., Lee, C. T., & Yu, J. Y. (2021). On the varying responses of east Asian winter monsoon to three types of El Niño: Observations and model hindcasts. *Journal of Climate*, *34*(10), 4089–4101. https://doi.org/10.1175/jcli-d-20-0784.1

Kim, J. W., & Yu, J. Y. (2020). Understanding reintensified multiyear El Niño events. *Geophysical Research Letters*, *47*(12), e2020GL087644. https://doi.org/10.1029/2020gl087644

Kim, J. W., & Yu, J. Y. (2021). Evolution of subtropical Pacific-onset El Niño: How its onset location controls its decay evolution. *Geophysical Research Letters*, *48*(5), e2020GL091345. https://doi.org/10.1029/2020gl091345

Kim, J. W., & Yu, J. Y. (2022). Single- and multi-year ENSO events controlled by pantropical climate interactions. *Npj Climate and Atmospheric Science*, *5*(1), 88. https://doi.org/10.1038/s41612-022-00305-y

Kug, J. S., Jin, F. F., & An, S. I. (2009). Two types of El Niño events: Cold tongue El Niño and warm pool El Niño. *Journal of Climate*, *22*(6), 1499–1515. https://doi.org/10.1175/2008jcli2624.1

21698996, 2023, 14, Downloaded from https://agupubs.onlinelibrary.wiley.com/doi/10.1029/2022JD038200 by University Of California - Irvine, Wiley Online Library on [21/08/2023]. See the Terms and Conditions (https://onlinelibrary.wiley.com/terms-and-conditions) on Wiley Online Library for rules of use; OA articles are governed by the applicable Creative Commons License

Large, W. G., & Danabasoglu, G. (2006). Attribution and impacts of upper-ocean biases in CCSM3. *Journal of Climate*, *19*(11), 2325–2346. https://doi.org/10.1175/jcli3740.1

Lee, J. W., Yeh, S. W., & Jo, H. S. (2019). Weather noise leading to El Niño diversity in an ocean general circulation model. *Climate Dynamics*, *52*(12), 7235–7247. https://doi.org/10.1007/s00382-016-3438-3

Lee, T., & McPhaden, M. J. (2010). Increasing intensity of El Niño in the central-equatorial Pacific. *Geophysical Research Letters*, *37*(14). https://doi.org/10.1029/2010gl044007

McGregor, S., Timmermann, A., Schneider, N., Stuecker, M. F., & England, M. H. (2012). The effect of the South Pacific convergence zone on the termination of El Niño events and the meridional asymmetry of ENSO. *Journal of Climate*, *25*(16), 5566–5586. https://doi.org/10.1175/jcli-d-11-00332.1

Mechoso, C. R., Robertson, A. W., Barth, N., Davey, M. K., Delecluse, P., Gent, P. R., et al. (1995). The seasonal cycle over the tropical Pacific in general circulation models. *Monthly Weather Review*, *123*(9), 2825–2838. https://doi.org/10.1175/1520-0493(1995)123<2825:tscott>2.0.co;2

Mudelsee, M. (2010). *Climate time series analysis: Classical statistical and bootstrap methods* (1st ed., p. 474). Springer.

Ohba, M., & Ueda, H. (2009). Role of nonlinear atmospheric response to SST on the asymmetric transition process of ENSO. *Journal of Climate*, *22*(1), 177–192. https://doi.org/10.1175/2008jcli2334.1

Okumura, Y. M., DiNezio, P., & Deser, C. (2017). Evolving impacts of multiyear La Niña events on atmospheric circulation and US drought. *Geophysical Research Letters*, *44*(22), 11–614. https://doi.org/10.1002/2017gl075034

Okumura, Y. M., Ohba, M., Deser, C., & Ueda, H. (2011). A proposed mechanism for the asymmetric duration of El Niño and La Niña. *Journal of Climate*, *24*(15), 3822–3829. https://doi.org/10.1175/2011jcli3999.1

Pacanowski, R. C., & Griffies, S. M. (1998). *MOM 3.0 manual* (p. 708). Geophysics Fluid Dynamics Laboratory.

Paek, H., Yu, J. Y., Hwu, J. W., Lu, M. M., & Gao, T. (2015). A source of AGCM bias in simulating the Western Pacific subtropical high: Different sensitivities to the two types of ENSO. *Monthly Weather Review*, *143*(6), 2348–2362. https://doi.org/10.1175/mwr-d-14-00401.1

Paek, H., Yu, J. Y., & Qian, C. (2017). Why were the 2015/2016 and 1997/1998 extreme El Niños different? *Geophysical Research Letters*, *44*(4), 1848–1856. https://doi.org/10.1002/2016gl071515

Philander, S. G. H., Gu, D., Halpern, D., Lambert, G., Lau, N.-C., Li, T., & Pacanowski, R. C. (1996). Why the ITCZ is mostly north of the equator. *Journal of Climate*, *9*(12), 2958–2972. https://doi.org/10.1175/1520-0442(1996)009<2958:wtiimn>2.0.co;2

Rayner, N. A. A., Parker, D. E., Horton, E. B., Folland, C. K., Alexander, L. V., Rowell, D. P., & Kaplan, A. (2003). Global analyses of sea surface temperature, sea ice, and night marine air temperature since the late nineteenth century. *Journal of Geophysical Research*, *108*(D14), 4407. https://doi.org/10.1029/2002jd002670

Saha, S., Moorthi, S., Wu, X., Wang, J., Nadiga, S., Tripp, P., et al. (2014). The NCEP climate forecast system version 2. *Journal of Climate*, *27*(6), 2185–2208. https://doi.org/10.1175/jcli-d-12-00823.1

Santoso, A., Mcphaden, M. J., & Cai, W. (2017). The defining characteristics of ENSO extremes and the strong 2015/2016 El Niño. *Reviews of Geophysics*, *55*(4), 1079–1129. https://doi.org/10.1002/2017rg000560

Stuecker, M. F. (2018). Revisiting the Pacific meridional mode. *Scientific Reports*, *8*(1), 1–9. https://doi.org/10.1038/s41598-018-21537-0

Sud, Y. C., Walker, G. K., & Lau, K. M. (1999). Mechanisms regulating sea-surface temperatures and deep convection in the tropics. *Geophysical Research Letters*, *26*(8), 1019–1022. https://doi.org/10.1029/1999gl900197

Tan, W., Wang, X., Wang, W., Wang, C., & Zuo, J. (2016). Different responses of sea surface temperature in the South China Sea to various El Niño events during boreal autumn. *Journal of Climate*, *29*(3), 1127–1142. https://doi.org/10.1175/jcli-d-15-0338.1

Timmermann, A., An, S. I., Kug, J. S., Jin, F. F., Cai, W., Capotondi, A., et al. (2018). El Niño–southern oscillation complexity. *Nature*, *559*(7715), 535–545. https://doi.org/10.1038/s41586-018-0252-6

Wang, C., Deser, C., Yu, J. Y., DiNezio, P., & Clement, A. (2017). El Niño and southern oscillation (ENSO): A review. *Coral Reefs of the Eastern Tropical Pacific*, 85–106.

Wang, C., & Wang, X. (2013). Classifying El Niño Modoki I and II by different impacts on rainfall in southern China and typhoon tracks. *Journal of Climate*, *26*(4), 1322–1338. https://doi.org/10.1175/jcli-d-12-00107.1

Wang, X., & Wang, C. (2014). Different impacts of various El Niño events on the Indian ocean Dipole. *Climate Dynamics*, *42*(3), 991–1005. https://doi.org/10.1007/s00382-013-1711-2

Weng, H., Behera, S. K., & Yamagata, T. (2009). Anomalous winter climate conditions in the Pacific rim during recent El Niño Modoki and El Niño events. *Climate Dynamics*, *32*(5), 663–674. https://doi.org/10.1007/s00382-008-0394-6

Wu, T. Y., Juang, H. M. H., Chen, Y. L., Liu, P. Y., Lin, S. I., Chen, J. H., & Lu, M. M. (2019). *CWB CFS 1-tier hindcast analysis and forecast verification* (Vol. 172). Climate Prediction S&T Digest.

Wu, X., Okumura, Y. M., Deser, C., & DiNezio, P. N. (2021). Two-year dynamical predictions of ENSO event duration during 1954–2015. *Journal of Climate*, *34*(10), 4069–4087. https://doi.org/10.1175/jcli-d-20-0619.1

Wu, X., Okumura, Y. M., & DiNezio, P. N. (2019). What controls the duration of El Niño and La Niña events? *Journal of Climate*, *32*(18), 5941–5965. https://doi.org/10.1175/jcli-d-18-0681.1

Wyrtki, K. (1985). Water displacements in the Pacific and the Genesis of El Niño cycles. *Journal of Geophysical Research*, *90*(C4), 7129–7132. https://doi.org/10.1029/jc090ic04p07129

Xie, S. P., & Philander, S. G. H. (1994). A coupled ocean-atmosphere model of relevance to the ITCZ in the eastern Pacific. *Tellus*, *46*(4), 340–350. https://doi.org/10.1034/j.1600-0870.1994.t01-1-00001.x

Xue, Y., Chen, M., Kumar, A., Hu, Z. Z., & Wang, W. (2013). Prediction skill and bias of tropical Pacific sea surface temperatures in the NCEP climate forecast system version 2. *Journal of Climate*, *26*(15), 5358–5378. https://doi.org/10.1175/jcli-d-12-00600.1

Yeh, S. W., Kug, J. S., & An, S. I. (2014). Recent progress on two types of El Niño: Observations, dynamics, and future changes. *Asia-Pacific Journal of Atmospheric Sciences*, *50*(1), 69–81. https://doi.org/10.1007/s13143-014-0028-3

Yeh, S. W., Wang, X., Wang, C., & Dewitte, B. (2015). On the relationship between the North Pacific climate variability and the central Pacific El Niño. *Journal of Climate*, *28*(2), 663–677. https://doi.org/10.1175/jcli-d-14-00137.1

Yu, J. Y. (2015). Precursors of ENSO beyond the tropical Pacific. *US CLIVAR Variations*, *13*(1), 15–20.

Yu, J. Y., & Fang, S. W. (2018). The distinct contributions of the seasonal footprinting and charged-discharged mechanisms to ENSO complexity. *Geophysical Research Letters*, *45*(13), 6611–6618. https://doi.org/10.1029/2018gl077664

Yu, J. Y., & Kao, H. Y. (2007). Decadal changes of ENSO persistence barrier in SST and ocean heat content indices: 1958–2001. *Journal of Geophysical Research*, *112*(D13). https://doi.org/10.1029/2006jd007654

Yu, J. Y., Kao, H. Y., & Lee, T. (2010). Subtropics-related interannual sea surface temperature variability in the central equatorial Pacific. *Journal of Climate*, *23*(11), 2869–2884. https://doi.org/10.1175/2010jcli3171.1

Yu, J. Y., & Kim, S. T. (2011). Relationships between extratropical sea level pressure variations and the central Pacific and eastern Pacific types of ENSO. *Journal of Climate*, *24*(3), 708–720. https://doi.org/10.1175/2010jcli3688.1

21698996, 2023, 14, Downloaded from https://agupubs.onlinelibrary.wiley.com/doi/10.1029/2022JD038200 by University Of California - Irvine, Wiley Online Library on [21/08/2023]. See the Terms and Conditions (https://onlinelibrary.wiley.com/terms-and-conditions) on Wiley Online Library for rules of use; OA articles are governed by the applicable Creative Commons License

Yu, J. Y., Lu, M. M., & Kim, S. T. (2012). A change in the relationship between tropical central Pacific SST variability and the extratropical atmosphere around 1990. *Environmental Research Letters*, *7*(3), 034025. https://doi.org/10.1088/1748-9326/7/3/034025

Yu, J. Y., & Mechoso, C. R. (1999). Links between annual variations of Peruvian stratocumulus clouds and of SST in the eastern equatorial Pacific. *Journal of Climate*, *12*(11), 3305–3318. https://doi.org/10.1175/1520-0442(1999)012<3305:lbavop>2.0.co;2

Yu, J. Y., Wang, X., Yang, S., Paek, H., & Chen, M. (2017). *The changing El Niño-Southern Oscillation and associated climate extremes* (pp. 1–38). John Wiley & Sons, Inc. https://doi.org/10.1002/9781119068020.ch1

Yu, J.-Y., & Zou, Y. (2013). The enhanced drying effect of Central-Pacific El Niño on US winter. *Environmental Research Letters*, *8*(1), 014019. https://doi.org/10.1088/1748-9326/8/1/014019

Yu, J.-Y., Zou, Y., Kim, S. T., & Lee, T. (2012). The changing impact of El Niño on US winter temperatures. *Geophysical Research Letters*, *39*(15). https://doi.org/10.1029/2012GL052483

Zheng, Z., Hu, Z. Z., & L'Heureux, M. (2016). Predictable components of ENSO evolution in real-time multi-model predictions. *Scientific Reports*, *6*(1), 1–9. https://doi.org/10.1038/srep35909

21698996, 2023, 14, Downloaded from https://agupubs.onlinelibrary.wiley.com/doi/10.1029/2022JD038200 by University Of California - Irvine, Wiley Online Library on [21/08/2023]. See the Terms and Conditions (https://onlinelibrary.wiley.com/terms-and-conditions) on Wiley Online Library for rules of use; OA articles are governed by the applicable Creative Commons License